Atmos. Chem. Phys. Discuss., https://doi.org/10.5194/acp-2018-609
Manuscript under review for journal Atmos. Chem. Phys.
Discussion started: 30 August 2018

Atmospheric Chemistry and Physics Discussions

The propagation of aerosol perturbations in convective cloud microphysics

Max Heikenfeld[1], Bethan White[1,2], Laurent Labbouz[1,3], and Philip Stier[1]

[1]Atmospheric, Oceanic & Planetary Physics, Department of Physics, University of Oxford, Oxford, United Kingdom
[2]School of Earth Atmosphere & Environment, Monash University, Melbourne, Australia
[3]Laboratoire d'Aérologie / CNES, Toulouse, France

Correspondence: Max Heikenfeld (max.heikenfeld@physics.ox.ac.uk)

Abstract. The impact of aerosols on ice- and mixed-phase processes in deep convective clouds remains highly uncertain and the wide range of interacting microphysical processes are still poorly understood. To understand these processes, we analyse diagnostic output of all individual microphysical process rates for two cloud microphysics schemes in the Weather and Research Forecasting model (WRF). We investigate the response of individual processes to changes in aerosol conditions and the propagation of perturbations through the microphysics all the way to the macrophysical development of the convective clouds. We perform simulations for two different cases of idealised supercells using two double-moment bulk microphysics schemes and a bin microphysics scheme. We use simulations with a comprehensive range of values for cloud droplet number concentration (CDNC) and cloud condensation nuclei (CCN) concentration as a proxy for aerosol effects on convective clouds. We have developed a new cloud tracking algorithm to analyse the morphology and time evolution of individually tracked convective cells in the simulations and their response to the aerosol perturbations.

This analysis confirms an expected decrease in warm rain formation processes due to autoconversion and accretion for polluted conditions. The height at which the freezing occurs increases with increasing CDNC. However, there is no evidence of a significant increase in the total amount of latent heat release from freezing and riming. The cloud mass and the altitude of the cloud centre of gravity show contrasting responses to changes in proxies for aerosol number concentration between the different microphysics schemes.

1 Introduction

Deep convective clouds are an important feature of the Earth's atmosphere, ranging from widespread convection dominating the atmosphere in the tropics to mid-latitude convective systems (Emanuel, 1994). The impact of aerosols on ice- and mixed-phase processes in convective clouds remains highly uncertain (Tao et al., 2012; Varble, 2018), which has implications for determining the role of aerosol-cloud interactions in the climate system. Representing these effects in global climate models poses additional challenges due to the relatively small length scales often less than a few kilometres at which convective clouds develop and because of limitations in the representations of microphysical processes in the convective parametrisations (Stocker, 2014; Tao et al., 2012; Sullivan et al., 2016) with only few models explicitly representing the effects of aerosols on deep convective clouds (e.g. Kipling et al., 2017; Labbouz et al., 2018; Zhang et al., 2017; Song and Zhang, 2011; Guo et al.,

2015). The highly localised nature of convective processes also leads to major challenges in observations both from satellites and aircraft measurements (Rosenfeld et al., 2014).

Over recent years numerous studies using cloud resolving model simulations (CRM) have investigated aerosol-convection interactions in various setups, ranging from case study simulations to idealised simulations of e.g. squall lines or supercells like the one used in this study (Kalina et al., 2014; Seifert and Beheng, 2006; Morrison, 2012; Storer et al., 2010). The results, however, vary strongly between many of these studies. The differences can be attributed to the simulation of different types of convection, different environmental conditions like humidity or wind shear, but are also related to differences between the models or modelling approaches used (Tao et al., 2012; Fan et al., 2016; White et al., 2017). These challenges in modelling are strongly related to numerous interacting physical processes (Fan et al., 2016) in the cloud microphysics and to the interaction between clouds and other processes in the atmosphere on different scales (Tao et al., 2012).

Convective invigoration (Andreae et al., 2004; Rosenfeld et al., 2008; Lebo and Seinfeld, 2011) has been proposed as a mechanism by which aerosols impact development of deep convective clouds. A higher number concentration of aerosols suitable to act as cloud condensation nuclei (CCN) can lead to more but smaller cloud droplets, which are less likely to be processed into rain and precipitated out of the cloud. This would lead to more water reaching the freezing level in the cloud where subsequent freezing leads to additional latent heating in the higher levels of the cloud, enhancing the strength of the convection with higher updraft speeds and cloud top height. Other studies point out the additional impact of the larger number of aerosols, and subsequently cloud droplets, leading to smaller ice particles which then favours increased cloud fraction, cloud top height, and cloud thickness (Fan et al., 2013) due to reduced fall speeds of the ice particles. This implies a significant radiative effect on the climate system through enhanced anvils (Koren et al., 2010). Grabowski and Morrison (2016) argue that the effects can be purely attributed to the effects of smaller droplets and ice crystals with negligible effects of the thermodynamic enhancement proposed in Rosenfeld et al. (2008). Some of the differences in the assessments of convective invigoration due to aerosols are actually caused by the difference in the definition of both changes in aerosol and the quantification of the strength of convection based on different variables such as surface precipitation, updraft speeds or cloud top heights (Lebo et al., 2012; Altaratz et al., 2014). Significant mechanisms buffering the impact of aerosols on clouds and precipitation, both with a focus on warm-phase processes (Stevens and Feingold, 2009) and for mixed-phase and ice-clouds (Fan et al., 2016) have been proposed. However, there are recent studies questioning the attribution of observed relationships between aerosol concentrations and cloud-top height to aerosol microphysical effects (Varble, 2018). Many studies have pointed out the representation of cloud microphysics in models as one of the main sources of uncertainty in high-resolution model studies of aerosol-cloud interactions or cloud feedbacks to a warming climate, especially for mixed-phase and ice-phase clouds (Khain et al., 2015; White et al., 2017; Tao et al., 2012). This also holds for the role of the microphysics schemes in global model simulations of both convection and aerosol-cloud interactions (Gettelman, 2015; Lohmann and Feichter, 2005; Malavelle et al., 2017).

Most currently used cloud microphysics schemes can be separated into two approaches (Khain et al., 2015). Bulk microphysics schemes assume a specific size distribution for a range of different hydrometeor classes and describe their evolution and interactions based on a certain number of moments of these distributions. Double moment schemes with both prognostic mass and number concentrations of the hydrometeors are the current standard and necessary to meaningfully represent aerosol-cloud

interactions (Khain et al., 2015; Igel et al., 2014). Bin microphysics schemes represent the different hydrometeors in the cloud through a number individual size bins per hydrometeor class, thus allowing for more flexible representation of the actual size distribution and the interaction between the different size bins (Khain et al., 2015). Due to the large number of simulated variables, however, this approach results in high computational cost. One of the main benefits is avoiding the artificial separation between cloud droplets and rain drops that causes challenges in bulk microphysics scheme for example in the form of a parametrisation of the autoconversion processes (Khain et al., 2015).While many studies have proposed that bin resolving microphysics schemes are necessary to reliably represent possible microphysical aerosol effects on convective clouds (Khain et al., 2004; Fan et al., 2016, 2012) in model simulations, a large range of studies and applications, e.g. routine numerical weather prediction (NWP), coupled simulations with a complex aerosol- and chemistry and global climate model simulations as well as a large number of CRM based studies of aerosol cloud interactions apply bulk microphysics schemes.

Glassmeier and Lohmann (2016) investigated the microphysical pathways of precipitation susceptibility to aerosols in the double-moment microphysics scheme from Seifert and Beheng (2006) analytically based on the microphysical rate equations. They found clear relationships for warm rain processes, but a more complicated picture once mixed- and ice-phase processes occur, due to compensating effects of aerosol perturbations on warm and ice-phase processes. These effects cannot be derived theoretically from the microphysical equations due to the complex interactions of different processes and links to dynamical changes (Glassmeier and Lohmann, 2016).

This study aims to unravel the underlying microphysical mechanisms responsible for the large diversity of simulated aerosol effects on convection through a comprehensive analysis of the propagation of aerosol perturbations through microphysical pathways in different microphysics schemes. We have implemented detailed microphysical process rate diagnostics for pathway analysis in the two double-moment microphysics schemes of Morrison et al. (2009) and Thompson et al. (2004). We analyse the cloud morphology and the spatial structure of the microphysical processes in individual tracked convective cells. Tracking individual convective cells in the simulation makes it possible to draw direct conclusions about the behaviour of individual convective cells in the simulations e.g. regarding their time evolution or the response to changes in simulation parameters that go beyond the bulk average over the simulation domain or the sum of all cloudy areas in the simulation. The analysis of tracked cumulus clouds has been applied in a number of studies (e.g Heus and Seifert, 2013; Dawe and Austin, 2012; Heiblum et al., 2016a, b) with a focus on various aspects of convective clouds including the effects of aerosol perturbations on deep convection (Terwey and Rozoff, 2014).

Furthermore, we derive averaged properties over the cloud life cycle. Our approach goes beyond previous studies with a similar setup (Morrison et al., 2009; Kalina et al., 2014) that mainly focussed on domain average properties and only a specific subset of microphysical processes. We display the microphysical process rates in the form of scaled pie charts. This has been inspired by previous studies using this type of visualisation of the spatio-temporal development of physical processes for other applications: Schutgens and Stier (2014) performed a pathway analysis for the aerosol processes in a global climate model (ECHAM-HAM). Chang et al. (2015) applied a microphysical pathway analysis including a similar visualisation of process rates to simulations of pyro-convective clouds, however, using a much simpler two-dimensional model for highly idealised individual clouds.

Atmos. Chem. Phys. Discuss., https://doi.org/10.5194/acp-2018-609
Manuscript under review for journal Atmos. Chem. Phys.
Discussion started: 30 August 2018

Atmospheric Chemistry and Physics Discussions

To isolate the impact of the cloud microphysical pathways, we represent idealised aerosol perturbations as a fixed cloud droplet number concentration in each simulation with the two bulk microphysics scheme and then perform simulations for a comprehensive range of these values for each microphysics scheme. The simulations in this study are performed for a well-documented idealised supercell setup (e.g. Weisman and Klemp, 1982, 1984; Morrison et al., 2009). This type of simulation is chosen to create a well-defined development of a strong convective cell, allowing us to focus purely on the microphysical evolution of individual isolated convective cells. To test the sensitivity of our results to environmental conditions, we include simulations of a different idealised supercell case described in Naylor and Gilmore (2012); Dawson et al. (2013); Kumjian et al. (2010). We compare the results to simulations performed with a bin microphysics scheme (HUJI spectral bin scheme) for different values of a fixed condensation nuclei concentration.

2 Methods

2.1 Model Setup

The simulations are performed with the Weather and Research Forecasting model (WRF) version 3.7.1 (Skamarock et al., 2005). We use the two-moment microphysics schemes from Thompson et al. (2004, 2008), denoted as THOM, and from Morrison et al. (2005, 2009), called MORR in our figures and tables. To isolate the impact of microphysical pathways we apply a fixed cloud droplet number concentration (CDNC) for each simulation. CDNC is varied between different simulations as a proxy for aerosol number concentrations. To investigate the differences between bulk- and bin cloud microphysics schemes, we also include additional simulations with the Hebrew University cloud model (HUCM) spectral-bin microphysics scheme (Khain et al., 2004; Lynn et al., 2005a, b), called SBM in the rest of the paper, varying the number of cloud condensation nuclei (CCN). We use the full version of the spectral bin microphysics scheme in WRF (Khain et al., 2011, 2012). Both bulk microphysics schemes make use of saturation adjustment, removing all water vapour exceeding the saturation vapour pressure in each time-step and instantaneously condensing it to cloud water at each timestep. This prevents a build-up of supersaturation in strong updrafts and can thus impact effects of perturbations in the microphysics (Lebo et al., 2012). The bin microphysics scheme (SBM) includes an explicit calculation of supersaturation in the microphysics at each timestep and allows for a build-up of supersaturation in strong updrafts over several timesteps.

We simulate two different idealised supercell cases. The first set of simulations (CASE1) is based on the default WRF quarter-circle shear supercell case (Khain and Lynn, 2009; Lebo and Seinfeld, 2011). An initial perturbation in the form of a warm bubble is applied to an initial sounding and wind shear forcing described in Weisman and Klemp (1982, 1984). This type of setup has been used for a number of similar studies in the past (Kalina et al., 2014; Storer et al., 2010; Morrison and Milbrandt, 2010). To test the robustness of our results across two different cases of idealised deep convection, a set of simulations for a second supercell case (CASE2) is based on observations and model setups from Naylor and Gilmore (2012); Dawson et al. (2013); Kumjian et al. (2010). This case features a significantly drier initial profile and forcing from convergence near the surface. Both idealised cases are simulated without a boundary layer scheme or calculation of surface fluxes or radiation.

The horizontal grid spacing of the simulation is 1 km to resolve the main features of the simulated supercell and we use a

Atmos. Chem. Phys. Discuss., https://doi.org/10.5194/acp-2018-609
Manuscript under review for journal Atmos. Chem. Phys.
Discussion started: 30 August 2018

Atmospheric Chemistry and Physics Discussions

model domain of 84 grid cells in each horizontal dimension. The vertical resolution of the 96 model layers varies from about 50 m at the surface to 300 m at the top of the model. Simulations are performed with a time-step of 5 seconds. The standard model diagnostics and the microphysical pathway diagnostics (Section 2.3) are output every 5 minutes to sufficiently resolve the development of the microphysical processes during the life cycle of the deep convective clouds.

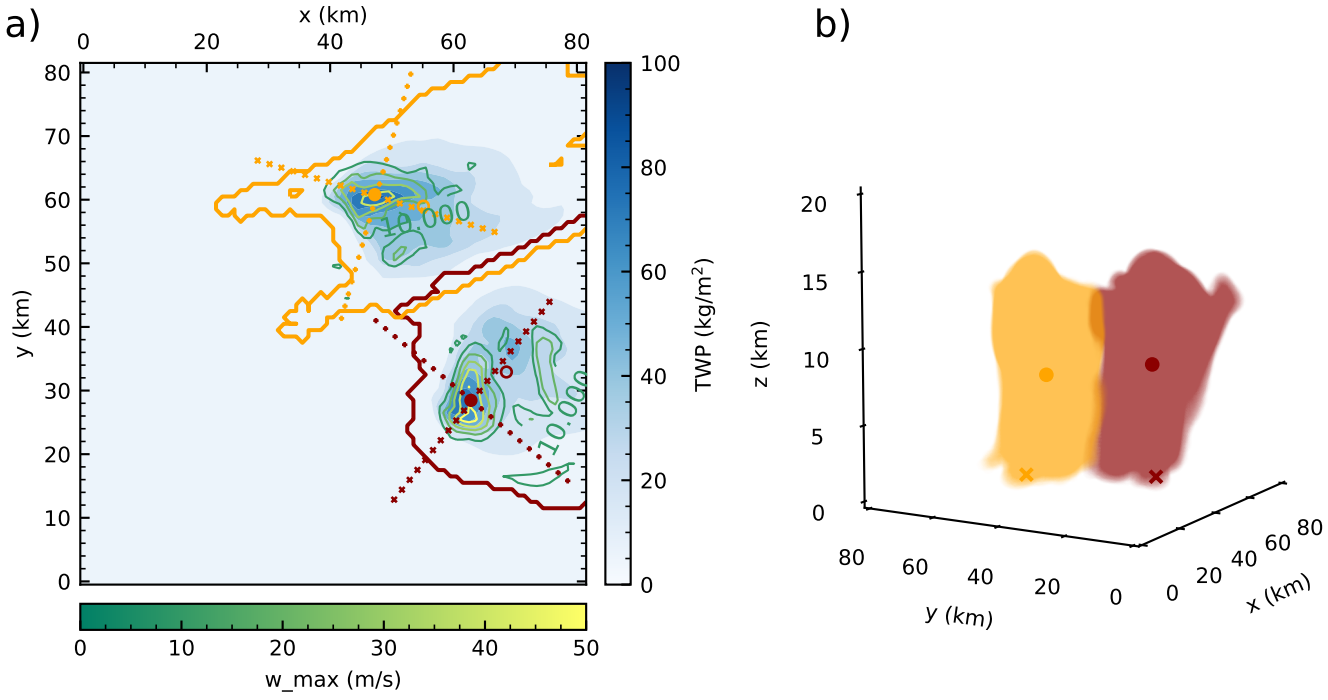

Figure 1. a) Illustration of the result of the tracking and watershedding methodology after 90 minutes of simulation time with the total water path field in blues and contours of column maximum vertical velocities in greens. The filled circles represent the tracked updraft cores, while the empty circles show the position of the centre of gravity determined by the watershedding algorithm. Crosses denote the slice along/across the line of travel of the cell that are used for the analysis of the cloud morphology. The coloured contour lines represent the projection of the respective cloud mask for each cell to the surface. b) 3D rendering of the 1 g kg^{-1} condensate mixing ratio threshold of the two tracked cells in the simulation at the same point in time including the horizontal location of the tracked updraft (cross) and centre of gravity (dot).

2.2 Variation of aerosol proxies: CDNC or CCN

We analyse the effects of varying the cloud droplet number concentration (CDNC) in the two bulk microphysics scheme to isolate the impact of microphysical pathways. We use a CDNC of 250 cm^{-3} as a baseline simulation. Simulations are performed for two CDNC values corresponding to a cleaner environment than the baseline simulation (50 cm^{-3} and 100 cm^{-3}) and five values representing more polluted conditions (500 cm^{-3}, 1000 cm^{-3}, 1500 cm^{-3}, 2000 cm^{-3}and 2500 cm^{-3}).

Atmos. Chem. Phys. Discuss., https://doi.org/10.5194/acp-2018-609
Manuscript under review for journal Atmos. Chem. Phys.
Discussion started: 30 August 2018

Atmospheric Chemistry and Physics Discussions

For the simulations with the spectral-bin microphysics scheme, activation of aerosols to cloud droplets is calculated from a cloud condensation nuclei (CCN) spectrum following the equation $N_C = N_0 * S^k$, with the prognostic supersaturation S, the particle number concentration N_0 and an exponent k. The exponent is kept fixed at $k = 0.5$, while N_0 is varied in a range from 75 cm^{-3} to 6750 cm^{-3}. This yields cloud droplet number concentrations with median values spanning a similar range to those chosen for the two bulk microphysics schemes (Table 1).

Table 1. Overview of the 52 simulations performed in this study, including the two cases simulated and the different CDNC/CCN values for each of the microphysics schemes. The CDNC for the SBM simulations are the median values for gridpoints with a cloud water mixing ratio larger than 10 $\mathrm{g/, kg}^{-1}$.

Case	**Microphysics**	**CDNC** (cm^{-3})	**CCN** (cm^{-3})
CASE1 Weisman and Klemp (1982, 1984)	**MORR** Morrison et al. (2005, 2009)	**50, 100, 250, 500, 1000, 1500, 2000, 2500**	-
	THOM Thompson et al. (2004, 2008)	**50, 100, 250, 500, 1000, 1500, 2000, 2500**	-
	SBM Khain et al. (2004) Lynn et al. (2005a, b)	12, 28, 54, 128, 419, 648, 870, 1310, 1753, 2194	**67.5, 135, 270, 540, 1350 2025, 2700, 4050, 5400, 6750**
CASE2 Naylor and Gilmore (2012) Dawson et al. (2013) Kumjian et al. (2010)	**MORR** Morrison et al. (2005, 2009)	**50, 100, 250, 500, 1000, 1500, 2000, 2500**	-
	THOM Thompson et al. (2004, 2008)	**50, 100, 250, 500, 1000, 1500, 2000, 2500**	-
	SBM Khain et al. (2004) Lynn et al. (2005a, b)	12 ,25, 47, 171, 393 603, 819, 1239, 1657, 2078	**67.5, 135, 270, 540, 1350 2025, 2700, 4050, 5400, 6750**

2.3 Pathway analysis

We have extended two double-moment bulk microphysics schemes (Morrison et al., 2005, 2009; Thompson et al., 2004, 2008) in WRF 3.7.1 by writing detailed microphysical pathway diagnostics at each output time step. This includes all individual process rates for both hydrometeor mass and hydrometeor number mixing ratio as well as individual latent heating rates for the three phase transitions (liquid-vapour, liquid-ice, ice-vapour) and the hydrometeor mass and number tendencies for the individual hydrometeor classes (cloud water, rain, cloud ice, graupel, snow) are diagnosed at every output time step.

More detail on the individual microphysical process rates is given in the appendix (Table A1 for the Morrison microphysics scheme and in Table A2 for the Thompson microphysics scheme, respectively). For the analyses, the processes are grouped

into a consistent set of classes, e.g. by the contribution to the formation of specific hydrometeor types or the contribution to latent heating in the phase changes of water.

2.4 Convective cell tracking

We have developed a tracking algorithm focussed on the tracking of individual deep convective cells in CRM simulations, but flexible enough to be extended to other applications, e.g. simulations of shallow convection or based on geostationary satellite observations using brightness temperature data. The initial tracking of features is performed on the column maximum vertical velocity at each output time step using the python tracking library trackpy (Allan et al., 2016). These features are then filtered and linked to consistent trajectories. The trajectories are extrapolated to two additional output timesteps at the start and at the end to allow for the inclusion of both the initiation of the cell and the decaying later stages of the cell development. Based on these trajectories, a three-dimensional watershedding algorithm *morphology.watershed* from the python image processing package scikit-image (van der Walt et al., 2014) is applied to the total condensed water content field (mass mixing ratio of all hydrometeors) at each output timestep to infer the volume of the cloud associated with the tracked updraft. We use a threshold of $1\,\mathrm{g\,kg^{-3}}$ to define the core cloudy gridpoints in the simulations. A variation of this threshold by up to an order of magnitude to $0.1\,\mathrm{g\,m^{-3}}$ only showed minor changes to the results of the study. A separate watershedding is performed for both liquid water content (cloud droplets and rain drops) and ice water content (all ice hydrometeors). This allows for the determination of the centre of gravity and the mass, for the entire cloud as well as for the in-cloud liquid and frozen phase, respectively. The evolution of the centre of gravity has been studied mainly for warm convective clouds (e.g. Koren et al., 2009; Dagan et al., 2015, 2017, 2018) and with a focus on the warm phase of deep convective clouds (Chen et al., 2017). Microphysical process rates, latent heating rates and other cloud microphysical parameters such as hydrometeor mixing ratios are summed up for regularly-spaced altitude intervals in the volume of the individual cells to get representative profiles for each cloud. We interpolate the microphysical process rates and other variables used in the analysis to slices along and perpendicular to the line of travel of the cell (Fig. 1) to visualise and analyse the morphology of the cells for different simulation setups and at different stages of the cloud life cycle.

3 Results

3.1 Baseline simulations

The simulations with CDNC = $250\,\mathrm{cm^{-3}}$ for both microphysics schemes (Fig. 2 and Fig. 3) are used as a baseline simulation representative of intermediate aerosol loading. During the initial phase of the formation of the convective cloud in the simulation using the Morrison bulk microphysics scheme (Fig. 2 a,d,g), the two major microphysical processes are condensation to form cloud droplets and rain formation from these droplets, while the top of the cloud at around $7.5\,\mathrm{km}$ is already influenced by freezing and riming processes. The simulation with the Thompson microphysics scheme shows a similar development during the initial cloud stage (Fig. 3 a,d,g) . The initiation of freezing at the top of the cloud is slightly delayed in comparison to the

Atmos. Chem. Phys. Discuss., https://doi.org/10.5194/acp-2018-609
Manuscript under review for journal Atmos. Chem. Phys.
Discussion started: 30 August 2018

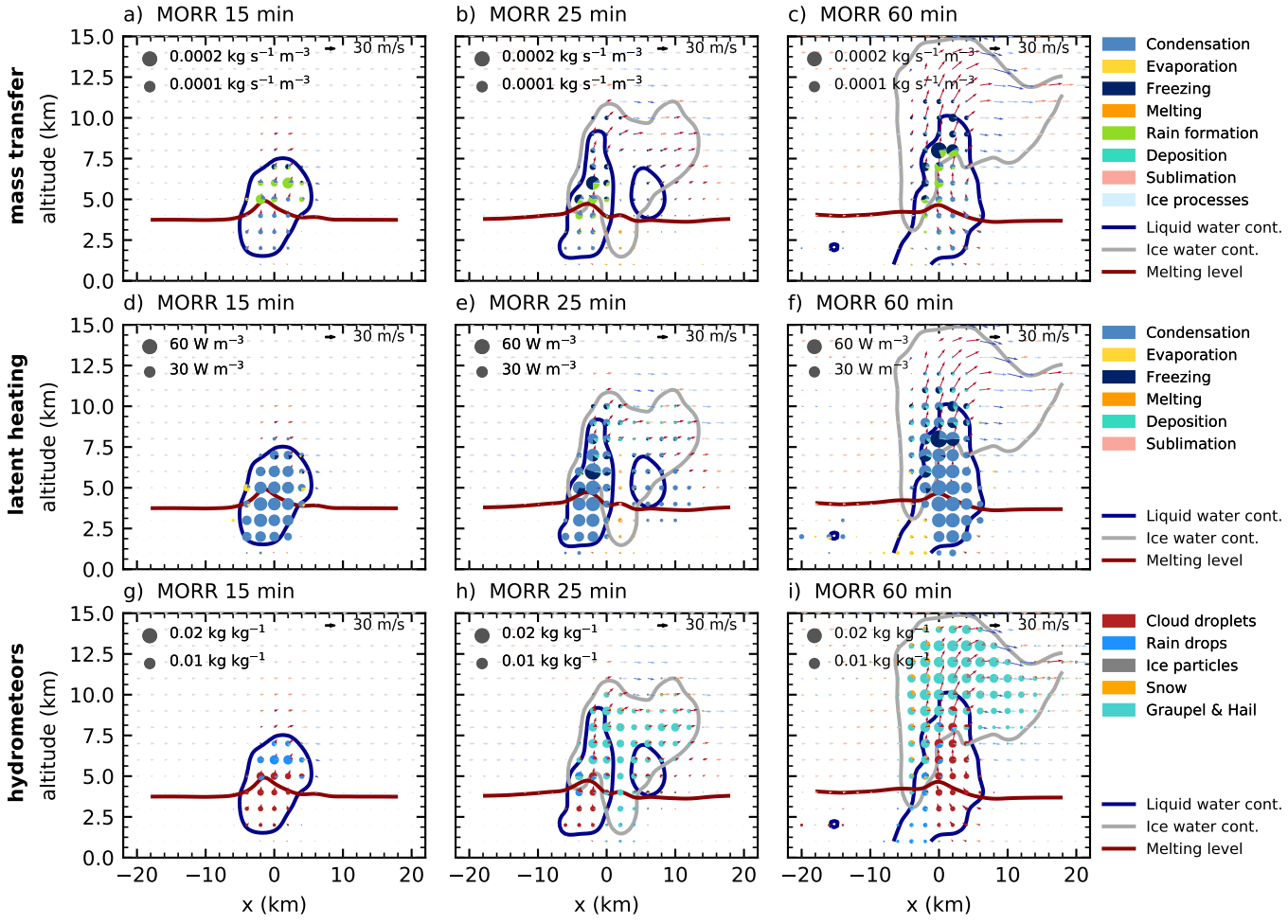

Figure 2. Cloud microphysical morphology along a slice parallel to the cell track for a cloud droplet number concentration of 250 cm^{-3} for the Morrison microphysics scheme. The area of each specific colour in the pie charts is proportional to the water turnover (a-c) in $\mathrm{kg\,m^{-3}\,s^{-3}}$ and latent heating (d-f) in $\mathrm{W\,m^{-3}}$ for the process rates and to the mass mixing ratio for the hydrometeors (g-i). Contour lines denote the mixing ratio threshold of 1 g/kg for liquid (blue) and ice (grey) content as well as the melting level (0°C isotherm). Arrows denote the wind field with updrafts in red and downdrafts in blue.

simulation with the Morrison scheme. During the next 10 minutes the cell quickly intensifies, dominated by the development of rain formation (autoconversion of cloud droplets and accretion of cloud droplets by rain) between 4 and 7 km. Freezing occurs at a height of about 7-8 km. After an hour of simulation, the cell has developed into a mature supercell with hail dominating the mass mixing ratio in the ice phase. A significant amount of cloud droplets extends up to 10 km height. Rain formation and freezing occur in the region of the strongest updraft with a width of about 5 km for both microphysics schemes. During the later

Atmos. Chem. Phys. Discuss., https://doi.org/10.5194/acp-2018-609
Manuscript under review for journal Atmos. Chem. Phys.
Discussion started: 30 August 2018

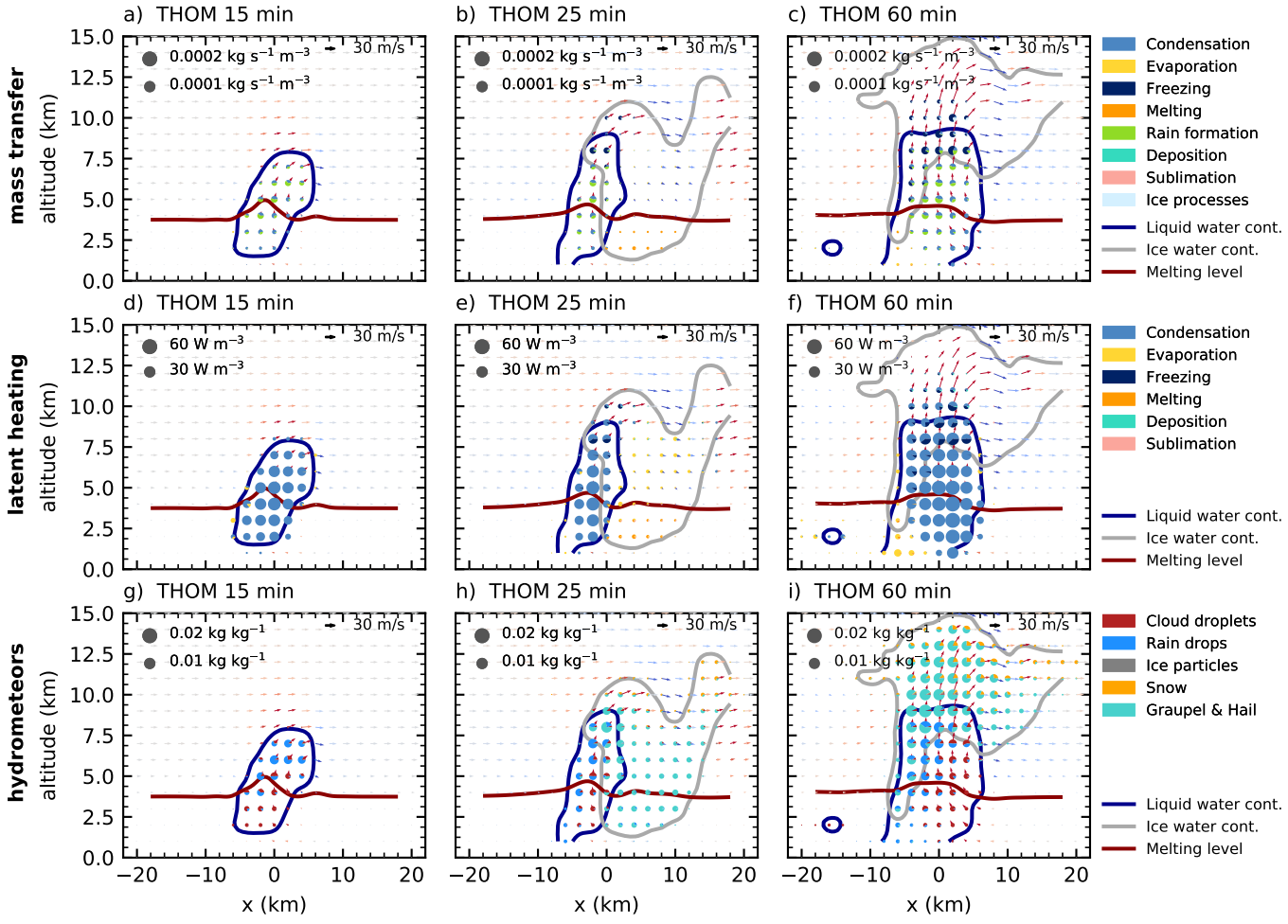

Figure 3. Cloud microphysical morphology along a slice parallel to the cell track for a cloud droplet number concentration of 250 cm^{-3} for the Thompson microphysics scheme as in Fig. 2.

stage, the freezing in the simulation using the Morrison microphysics scheme takes place in two distinct regions, one directly above the region where rain formation starts at about 6 km height and the other in a region at the top of the mixed-phase region of the cloud around 10 km height (Fig. 2 c). The Thompson scheme instead shows a more confined region of freezing. In both bulk microphysics schemes, condensation processes dominate the latent heat release in the cloud for all stages of the cloud development (Fig. 2 d-f, Fig. 3 d-f). In the mature stage of the cell, the main difference in the hydrometeor classes between the two microphysics schemes is an enhanced presence of snow both in the core and in the anvil for the Thompson microphysics scheme (Fig. 2 i and Fig. 3 i).

Atmos. Chem. Phys. Discuss., https://doi.org/10.5194/acp-2018-609
Manuscript under review for journal Atmos. Chem. Phys.
Discussion started: 30 August 2018

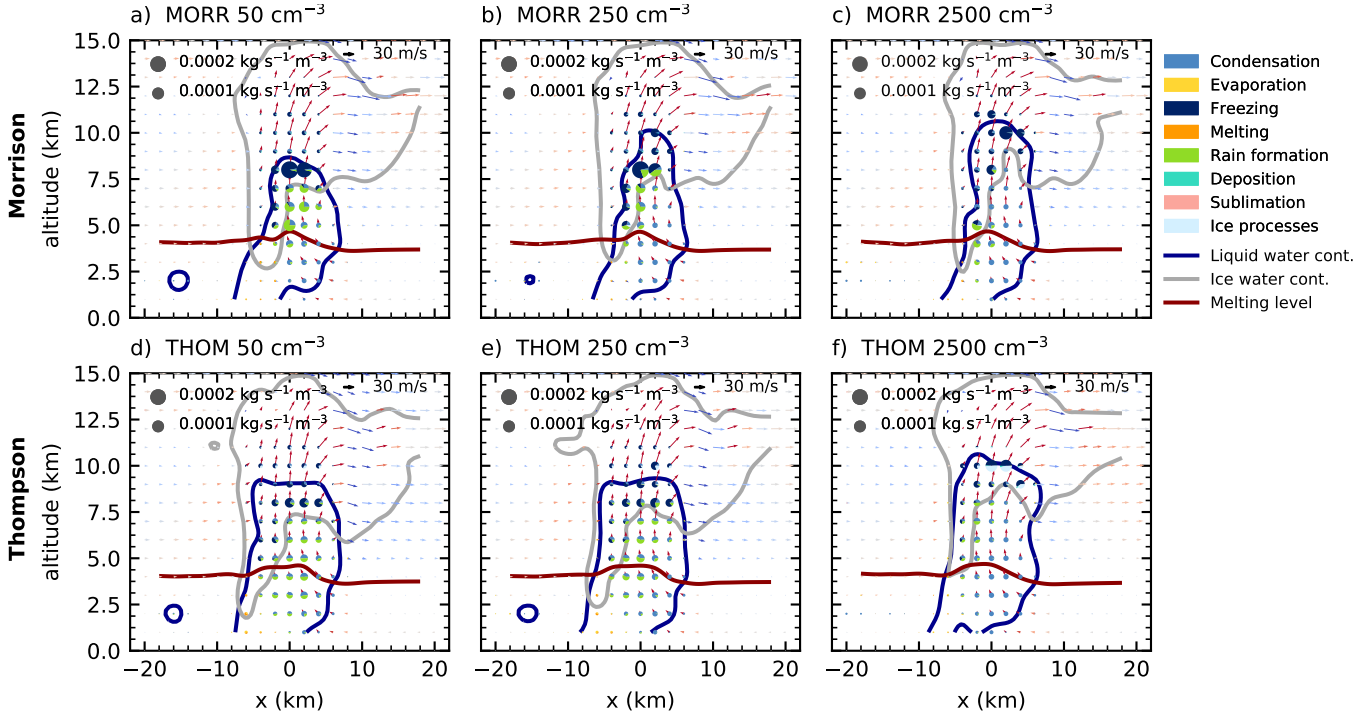

Figure 4. Cloud microphysical morphology along a slice through the cloud parallel to the track of the cell for simulations with three different CDNC values (left: 50 cm^{-3}, middle: 2500 cm^{-3},right: 2500 cm^{-3}) after 60 minutes of simulation using the two bulk microphysics schemes (top: Morrison, bottom: Thompson).

3.2 Effects on cloud morphology and microphysical process rates

We first investigate changes to the simulations from a variation of CDNC in the CASE1, based on Weisman and Klemp (1982, 1984). We focus on three different CDNC values (clean, baseline, polluted, see Fig. 4) after 60 minutes of simulations using the two bulk microphysics schemes. In the microphysical process rates, a decrease of rain formation from droplets (autoconversion and accretion) with increasing CDNC is evident in the core of the cell for both bulk microphysics schemes. For both bulk schemes, the freezing and riming processes are shifted upwards with increasing CDNC. The mixed phase region of the cloud, indicated by the liquid water mixing ratio contour in Fig. 4, extends about 1-2 km higher in the polluted case for each bulk scheme. In the hydrometeor mass mixing ratios (Fig. 5), an increase in cloud droplet mass at the expense of rain drops for increasing CDNC is evident in both bulk microphysics schemes and in the spectral bin microphysics scheme, particularly in the mixed phase region of the cloud at around 6-8 km). In the Thompson scheme most of the ice-phase hydrometeor mass is present in the form of snow for the high CDNC simulation (Fig. 5 d), especially towards the cloud top and in the anvil region, while graupel dominates except in the anvil for the cleanest case (Fig. 5 c). In contrast, the ice-phase in the Morrison scheme shows a high hail mixing ratio for low and high CDNC values (Fig. 5 a,b) and additional ice particles, but only small amounts

of snow in the simulation with the highest CDNC value. The simulations using the spectral bin microphysics scheme (Fig. 5 e,f) show a stronger increase in cloud droplets than the two bulk schemes for increased CCN. Graupel and hail, the predominant ice-phase hydrometeors in the cleanest simulation, get replaced by cloud ice particles for the highest CCN value. However, it has to be taken into account that the definition of the hydrometeor classes differs between the three different microphysics schemes, so this ambiguity could be responsible for some of the differences.

Fig. 6 provides an integrated view of the evolution of the microphysical process rates over the life cycle of the convective cloud following the track of the cell for the two bulk microphysics schemes. For both schemes, a strong decrease in the warm rain formation processes (autoconversion of cloud droplets and accretion of cloud droplets by rain) with increased CDNC can be observed. This even leads to a complete shut-down of warm rain production in the Thompson scheme, which is also evident in the absence of rain hydrometeors in Fig. 4. As a result, evaporation in the lowest model levels decreases strongly for the high CDNC value in the simulations with the Thompson scheme. The dominant region of freezing processes is lifted from around 8 km height in the low CDNC case to around 10 km for the high CDNC case height in both schemes. While deposition on ice hydrometeors is a significant process for all values of CDNC for the Morrison scheme, it becomes more enhanced for the most polluted simulation using the Thompson scheme, related to the change in the dominant ice-phase hydrometeor class to snow (Fig. 5). Condensation onto cloud droplets is present in all simulations up to 10 km height in comparable amounts and dominates the latent heating due to the large energy transfer involved. Deposition processes onto ice hydrometeors are significant for both the most clean and the most polluted simulation in the Morrison scheme, while the Thompson scheme shows much more deposition in the most polluted case, which can be related to the changes in the hydrometeor composition (Fig. 5). The decrease in the total amount of microphysical mass transfer in all simulations around 55 minutes into the simulations is caused by the splitting of the tracked cell into two individual cells. However, no significant change to the relative proportions of the different processes can be observed at this stage.

A more detailed analysis of the processes involved in the formation of rain over the lifetime of the cells (Fig. 7) reveals that autoconversion of cloud droplets to rain for the highest CDNC values in both bulk schemes is almost negligible, with only very little autoconversion in the Morrison scheme, even for the smallest CDNC value. Accretion of cloud droplets by rain is strongly depressed for high CDNC in both microphysics schemes. Melting of ice hydrometeors contributes significantly to the production of rain in both bulk schemes and is reduced for the high CDNC case, especially in the Thompson scheme.

The processes transforming liquid to frozen water can be further broken down into processes representing the freezing of individual cloud droplets or raindrops and riming processes, in which liquid water is accreted by existing ice-phase hydrometeors (Fig. 8). For both bulk microphysics schemes, freezing of rain drops and cloud droplets occur in two separate layers, with freezing of rain drops at around 8 km and freezing of cloud droplets above a height of 10 km up to 14 km. In both microphysics schemes, freezing of rain drops is strongly decreased for increased CDNC (Fig. 8 b,d), while freezing of cloud droplets is increased by about a factor of three. The riming processes are spread out over a much larger altitude range in the cloud, between the melting level at about 4 km and about 11 km height for riming of cloud droplets and below 9 km for the riming of rain drops. Riming is significantly stronger at all CDNC values in the simulations with the Morrison scheme (Fig. 8 a,b). In the Morrison scheme, riming of rain droplets is strongly decreased for higher CDNC and mainly restricted to around 5 km height.

Atmos. Chem. Phys. Discuss., https://doi.org/10.5194/acp-2018-609
Manuscript under review for journal Atmos. Chem. Phys.
Discussion started: 30 August 2018

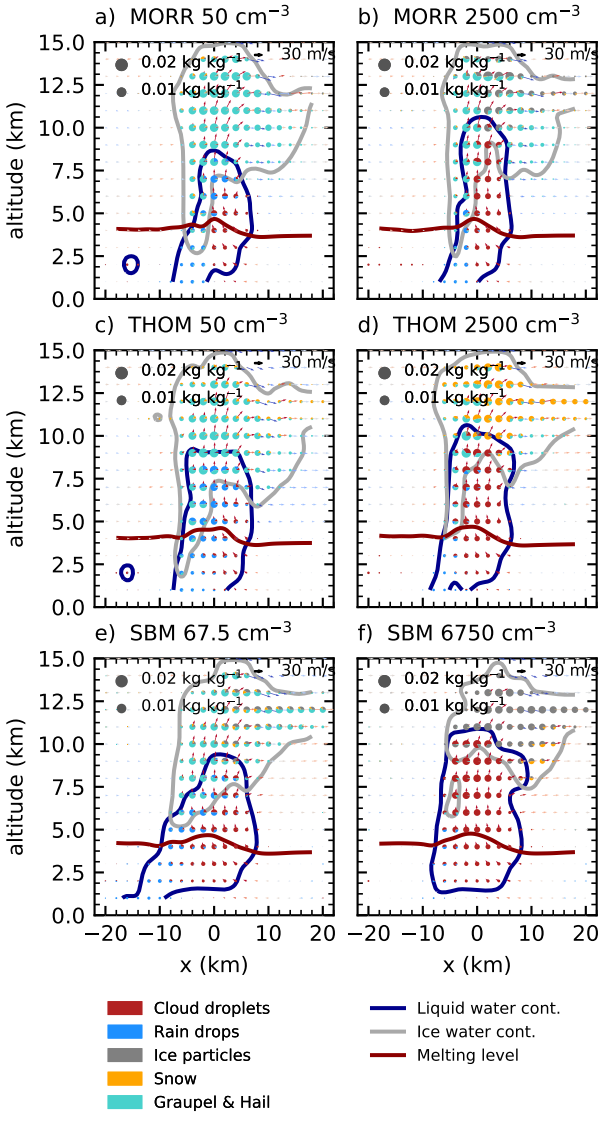

Figure 5. Hydrometeor mass mixing ratios in a slice along the line of travel of the cell for the most clean (left) and most polluted (right) simulations after 60 minutes of simulation for the three microphysics schemes in CASE1.

In the Thompson microphysics scheme (Fig. 8 c,d), rain drop riming is also strongly decreased for high CDNC, but still occurs over the same height range as in the low CDNC case. Both microphysics schemes show a slight increase in droplet riming with higher CDNC over the entire altitude range. We can thus explain the shift in freezing and riming processes observed in Fig. 6 by a decreased riming of rain droplets at lower altitudes and a shift from freezing rain drops to freezing of cloud droplets occurring at higher altitudes.

Latent heating constitutes a key feedback of the microphysics scheme onto the model dynamics along with changes to the

Atmos. Chem. Phys. Discuss., https://doi.org/10.5194/acp-2018-609
Manuscript under review for journal Atmos. Chem. Phys.
Discussion started: 30 August 2018

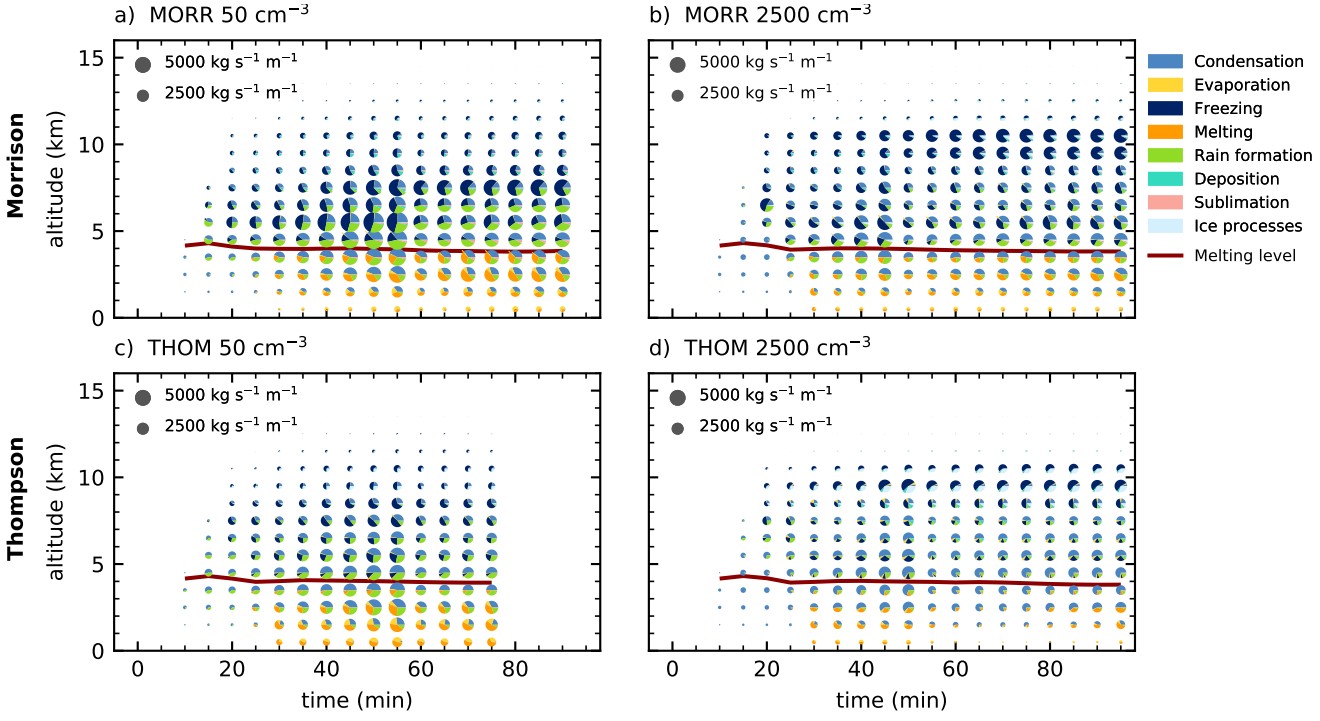

Figure 6. Time evolution of the microphysical process rates for the most clean (left) and most polluted (right) simulations and the two bulk microphysics schemes (Morrison: top, Thompson: bottom) in CASE1. The pie charts denote mass transfer summed up over the volume of the cloud in each altitude interval for the different groups of microphysical process rates with the area of each colour proportional to the mass transfer. The red line shows the height of the 0°C isotherm.

buoyancy due to changes in condensate loading. The total latent heating over the lifetime of the tracked cells in CASE1 is shown in Fig. 9 for all three microphysics schemes and split up into the individual phase changes for the two bulk microphysics schemes in Fig. 10.

Latent heat release from condensation is the dominant contribution to the latent heating and about a magnitude stronger than the other contributions, thus determining the general shape of the latent heating profile (Fig. 9 and Fig. 10 a,g). The changes to condensation due to changes in CDNC in the two bulk microphysics schemes are comparatively small, which can be explained by the use of saturation adjustment in the calculation of the condensation, which does not include an effect of changes in droplet radius onto the condensation and evaporation processes.

All three microphysics schemes show a small shift of latent heating to higher altitudes superimposed on that in the range between 7 km and about 10 km for increasing CDNC (Fig. 9), which can be associated with the shifts in freezing and riming Fig. 10 d,i), described in more detail in Fig. 8. The decrease in latent cooling from melting processes in the lowest layers is stronger in the Thompson scheme than in the Morrison scheme (Fig. 10 g,h).

There are stronger differences between the microphysics schemes in the latent heating and cooling from sublimation and de-

Atmos. Chem. Phys. Discuss., https://doi.org/10.5194/acp-2018-609
Manuscript under review for journal Atmos. Chem. Phys.
Discussion started: 30 August 2018

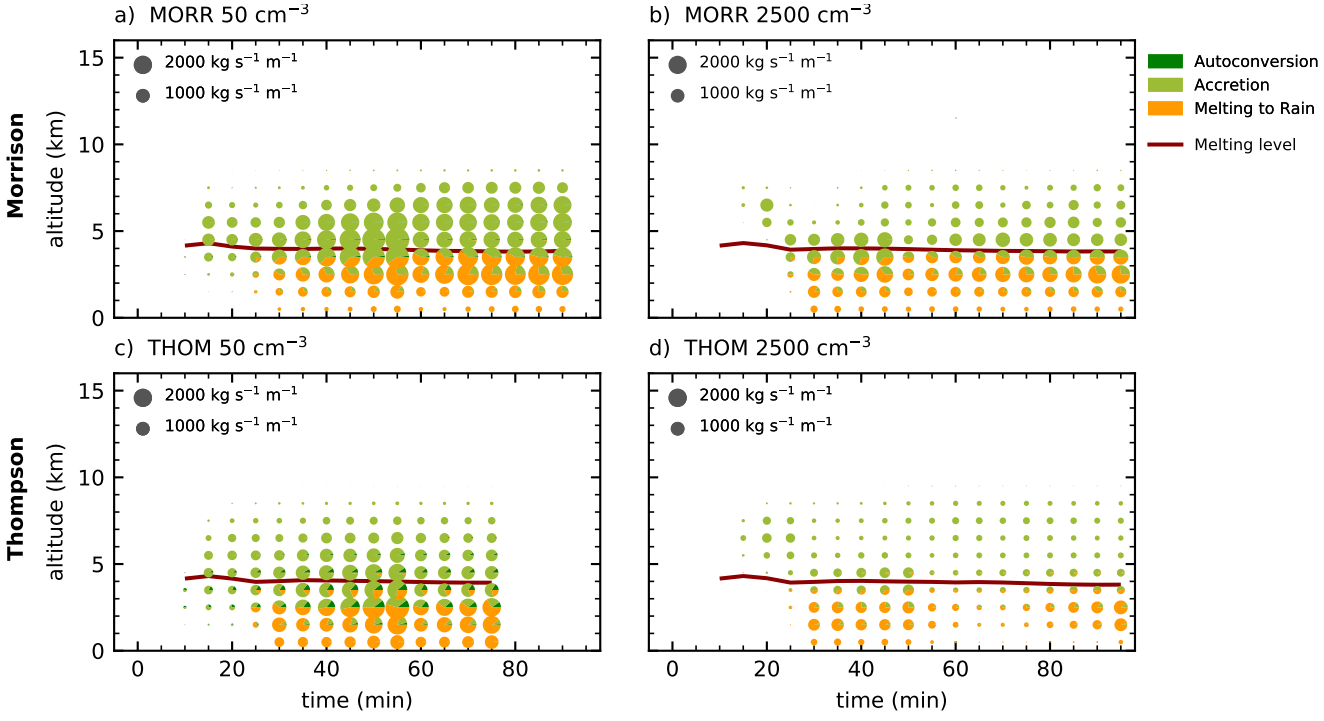

Figure 7. Time evolution of the microphysical process rates relevant for rain formation processes (autoconversion, accretion of cloud droplets by rain and melting of ice hydrometeors) as in Fig. 6.

position and the response to changes in CDNC. The Morrison scheme shows a significant decrease of both sublimation and deposition with increased CDNC (Fig. 10 e,f). In the Thompson scheme, however, higher CDNC leads to an increase in deposition in the higher parts of the cloud (Fig. 10 k) while sublimation of ice hydrometeors is weak and barely affected by changes in CDNC (Fig. 10 l) . This difference between the bulk microphysics schemes stems from the fact that deposition on graupel is not implemented in the Thompson scheme. That means that the decrease in graupel mixing ratio with higher CDNC (Fig 5) leads to an increase in deposition due to a higher abundance and thus higher deposition rates on ice and snow. In contrast, deposition onto hail is the dominant deposition component in the Morrison scheme and decreases as the hail gets replaced by ice and snow for higher CDNC values. The differences are in part caused by the Thompson scheme not allowing for deposition on graupel hydrometeors, which make up a large fraction of the ice phase and also show a strong change in their mixing ratio with a change in CDNC.

In contrast to the increased latent heating from freezing or melting, changes in condensation and evaporation as well as sublimation and deposition are linked to a change in condensate loading, which affects the buoyancy of the cloud and thus at least partially buffers the impact of latent heating and cooling on the dynamics of the clouds.

Atmos. Chem. Phys. Discuss., https://doi.org/10.5194/acp-2018-609
Manuscript under review for journal Atmos. Chem. Phys.
Discussion started: 30 August 2018

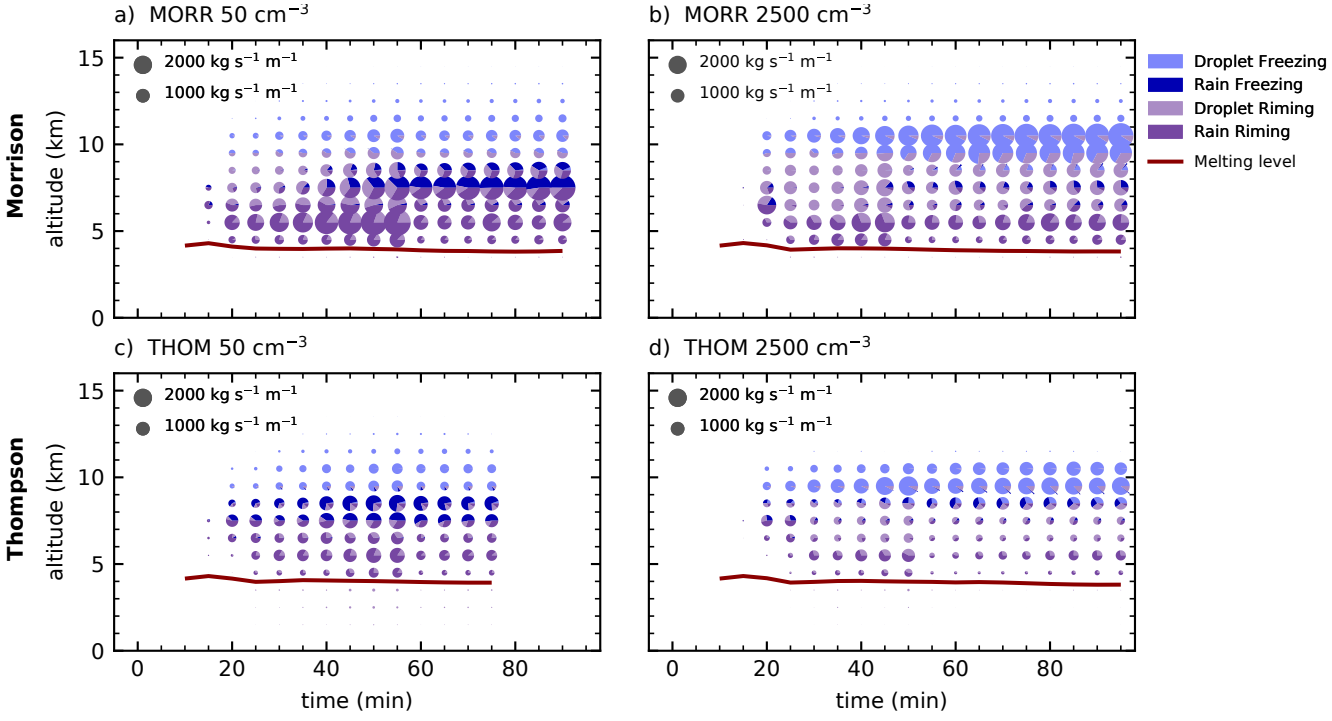

Figure 8. Time evolution of the the microphysical process rates of freezing and riming processes as in Fig. 6.

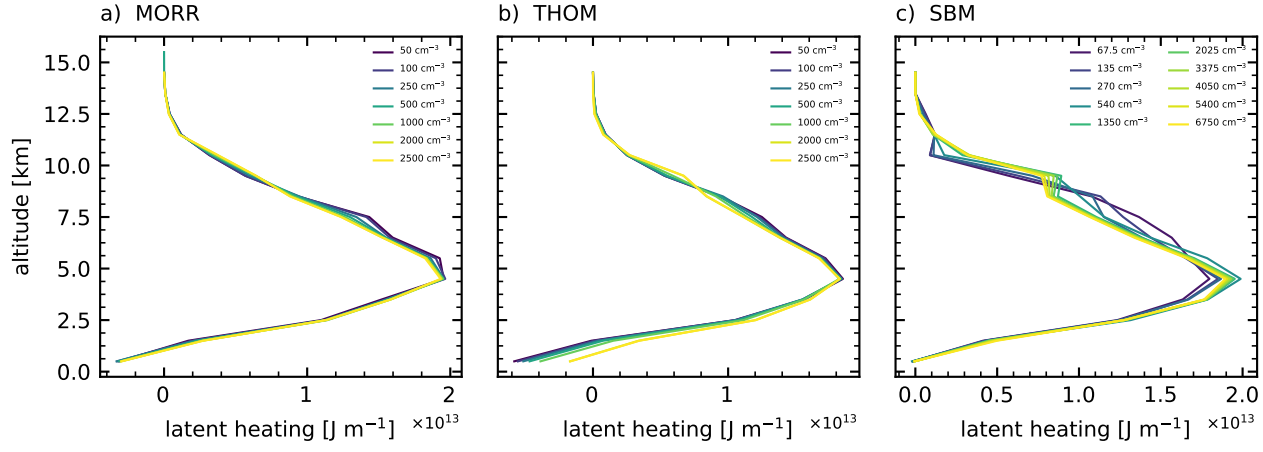

Figure 9. Profiles of the sum of latent heating over the lifetime of the dominant tracked cell for the three microphysics schemes in CASE1.

3.3 Effects on cloud mass and centre of gravity

The tracking and watershedding allows for a determination of the cloud mass inside the identified cloud volumes and the centre of gravity of the hydrometeors in the cloud. These analyses are also performed separately for the liquid-phase and ice-phase

Atmos. Chem. Phys. Discuss., https://doi.org/10.5194/acp-2018-609
Manuscript under review for journal Atmos. Chem. Phys.
Discussion started: 30 August 2018

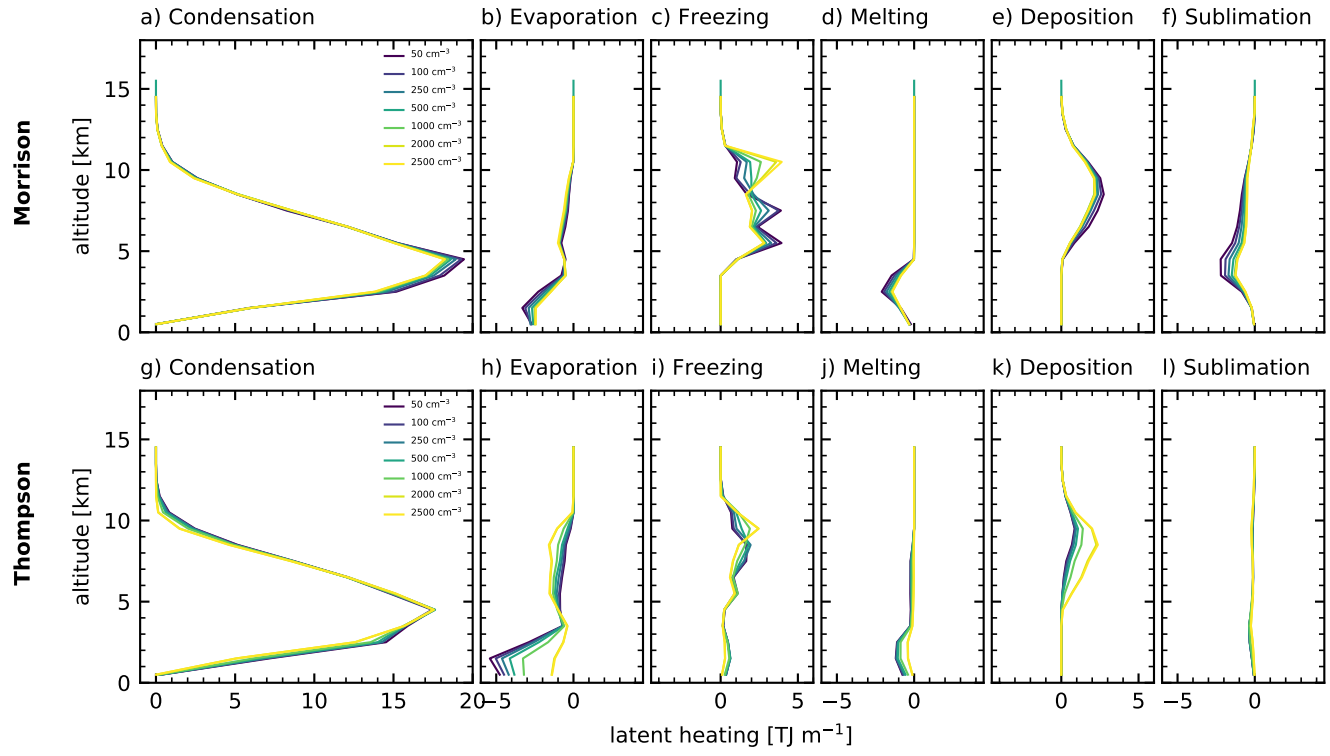

Figure 10. Profiles of the components of the latent heating and cooling over the lifetime of the tracked cell for the two bulk microphysics schemes in CASE1.

hydrometeors in the cloud, which allows us to relate the changes in the properties for the entire cloud to changes in the individual phases.

The evolution of the cloud mass and the mass of the water phases in the cloud (Fig. 11) in the three microphysics schemes is similar, with a maximum cloud mass of about $2{\cdot}10^{10}$ kg for all microphysics schemes, before the splitting of the cell and then about $1.5{\cdot}10^{10}$ kg for the two bulk microphysics schemes (Fig. 11 a,b) and slightly higher cloud masses of up to $1.8{\cdot}10^{10}$ kg in the spectral bin microphysics scheme (Fig. 11 c). The cloud mass and also the difference between the bulk schemes and the bin scheme are dominated by the ice-phase hydrometeors, while the liquid-phase mass is very similar in all three different microphysics schemes, making up about 20-25% of the total cloud mass. There are, however, marked differences in the response to changes of the aerosol proxy between the microphysics schemes. The Morrison scheme shows a decrease of total cloud mass and ice-phase mass by about 10-15% over the range in which we increase the CDNC and no significant changes in the liquid phase. In the Thompson scheme, however, increased CDNC leads to an increase in ice-phase and total mass and a small increase in cloud liquid mass. In the simulations using the SBM scheme, the two phases show a differing response to the aerosol proxy with more liquid hydrometeor mass and less ice-phase mass for increasing CCN.

The altitude of the centre of gravity is affected by the choice of microphysics scheme, with an overall higher centre of gravity

Atmos. Chem. Phys. Discuss., https://doi.org/10.5194/acp-2018-609
Manuscript under review for journal Atmos. Chem. Phys.
Discussion started: 30 August 2018

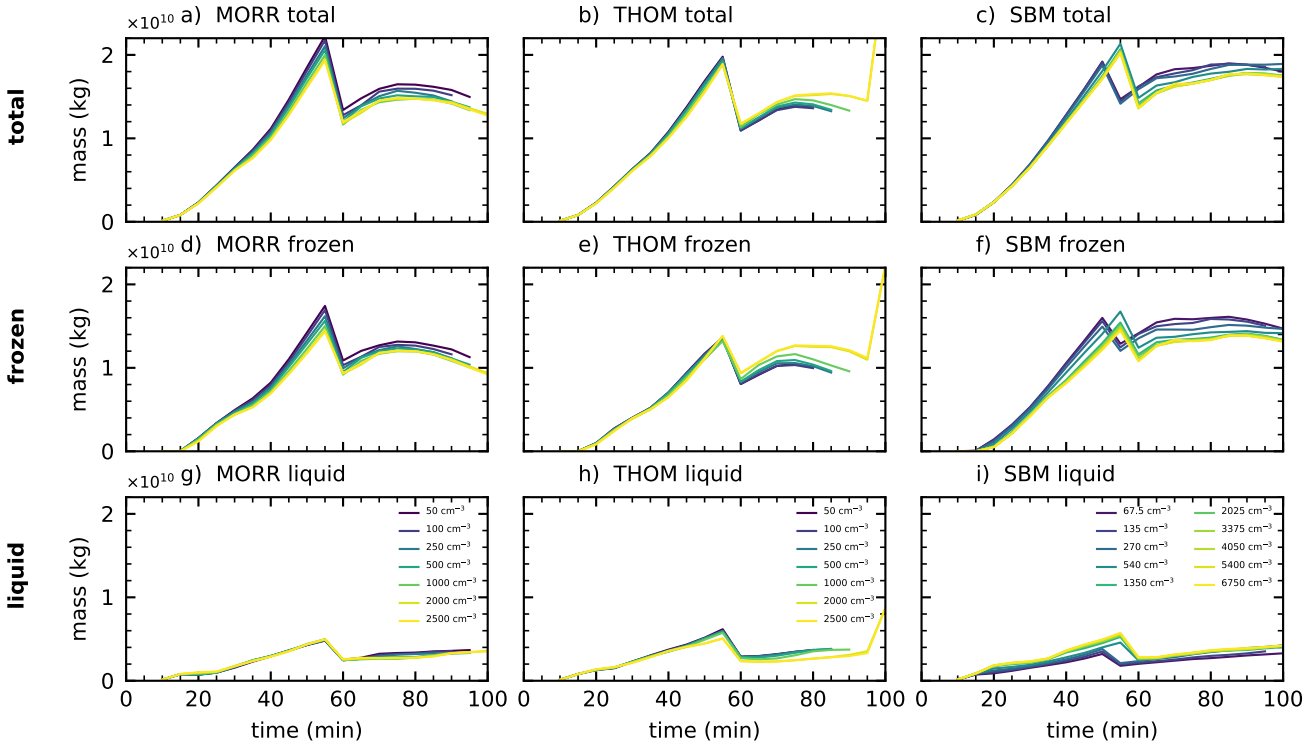

Figure 11. Total water mass, liquid water mass and ice water mass in the dominant tracked cell for the three different microphysics schemes (Morrison: left, Thompson: middle, SBM: right) in CASE1. The jump in the curves occurs at the point where the cell splits into two individual cells.

for the SBM scheme (Fig. 12 c) compared to the two bulk microphysics schemes (Fig. 12 a,b). There is a consistent response in the cloud heights for all three microphysics schemes. The two bulk microphysics schemes show an increase in the height of the centre of gravity of the entire cloud, which is more pronounced using the Thompson scheme (about 1.5 km) than in the Morrison scheme (about 0.5-1 km). This includes an upward shift in both the liquid and frozen water in the cloud for both bulk microphysics schemes. The simulations with the spectral bin microphysics scheme (SBM) show a significant increase in the height of the liquid phase of the cloud with increased CCN. The ice-phase mass and the total cloud mass, are also centred about 1 km higher for the most polluted case compared to the cleanest case.

All three microphysics schemes show a clear saturation in the effect of changes in the CDNC/CCN concentration. Variations above 2000 cm^{-3} in the bulk schemes and above 1350 cm^{-3} in the SBM simulation only lead to insignificant effects on both the cloud mass and the altitude of the centre of gravity of the different phases.

Atmos. Chem. Phys. Discuss., https://doi.org/10.5194/acp-2018-609
Manuscript under review for journal Atmos. Chem. Phys.
Discussion started: 30 August 2018

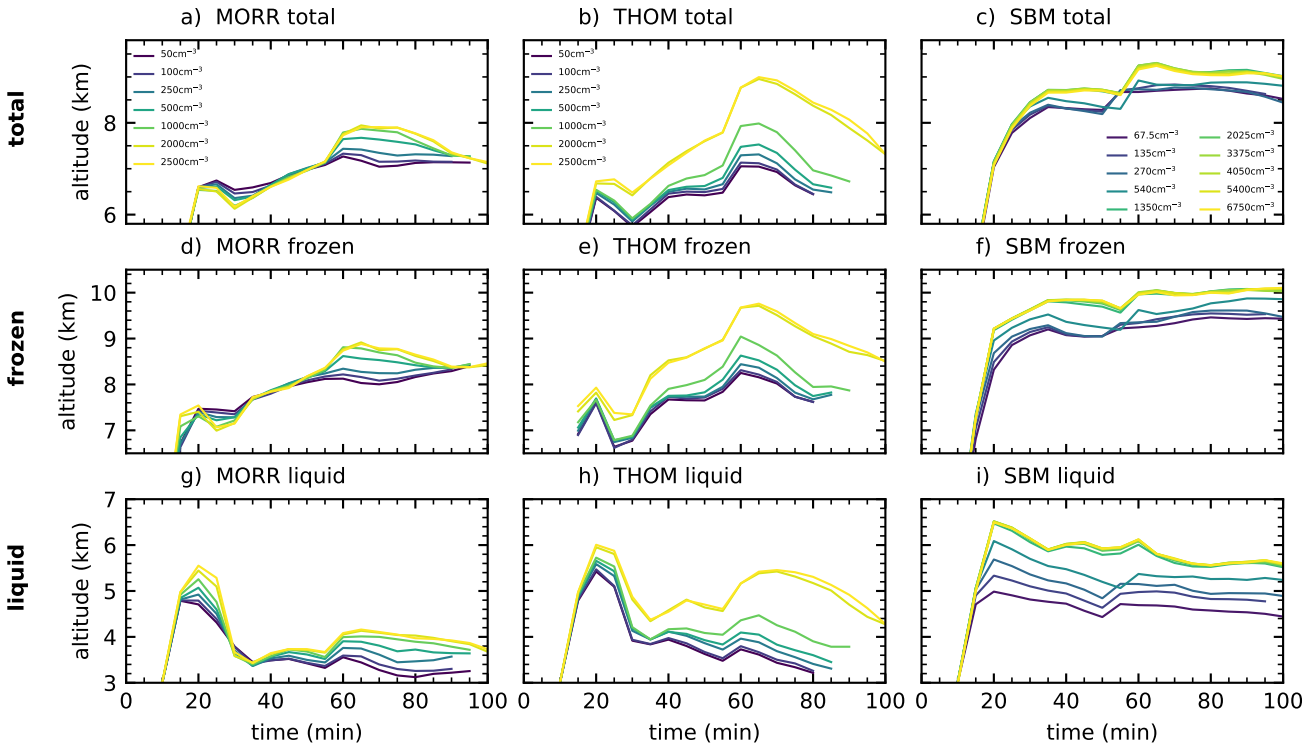

Figure 12. Altitude of the centre of gravity of the cloud and the individual phases for the three different microphysics schemes (Morrison: left, Thompson: middle, SBM: right) in CASE1.

3.4 Sensitivity test: a second idealised supercell case (CASE2)

To investigate the representativeness of the results and the response of the deep convective clouds to the variation of aerosol proxies CDNC and CCN, the same set of simulations and analyses have been performed for a second idealised supercell case (CASE2) with different forcing and initial conditions (Section 2.1). When looking at the time evolution of the cloud averaged process rates for the two bulk microphysics schemes (Fig. 13), it is obvious that the total microphysical water transfer is much weaker in CASE2 than in CASE1, with process rates about a factor of three smaller. This case shows much stronger differences between the two bulk microphysics schemes in the general evolution of convection. For the Morrison microphysics scheme a development of the convective cloud in two stages occurs. After an initial maximum in the microphysical processes after around 30 minutes of simulation time, the convective activity becomes weaker before picking up again after about an hour of simulation time. For the Thompson microphysics scheme, this second episode of development in the tracked cell is completely absent for all simulations, with the cloud dissipating after about 60 minutes of simulation time. However, the shifts in the microphysical processes due to a variation of CDNC are similar to the effects seen for the previous case for both microphysics schemes. The formation of rain due to autoconversion of cloud droplets and accretion by rain is smaller and restricted to lower

Atmos. Chem. Phys. Discuss., https://doi.org/10.5194/acp-2018-609
Manuscript under review for journal Atmos. Chem. Phys.
Discussion started: 30 August 2018

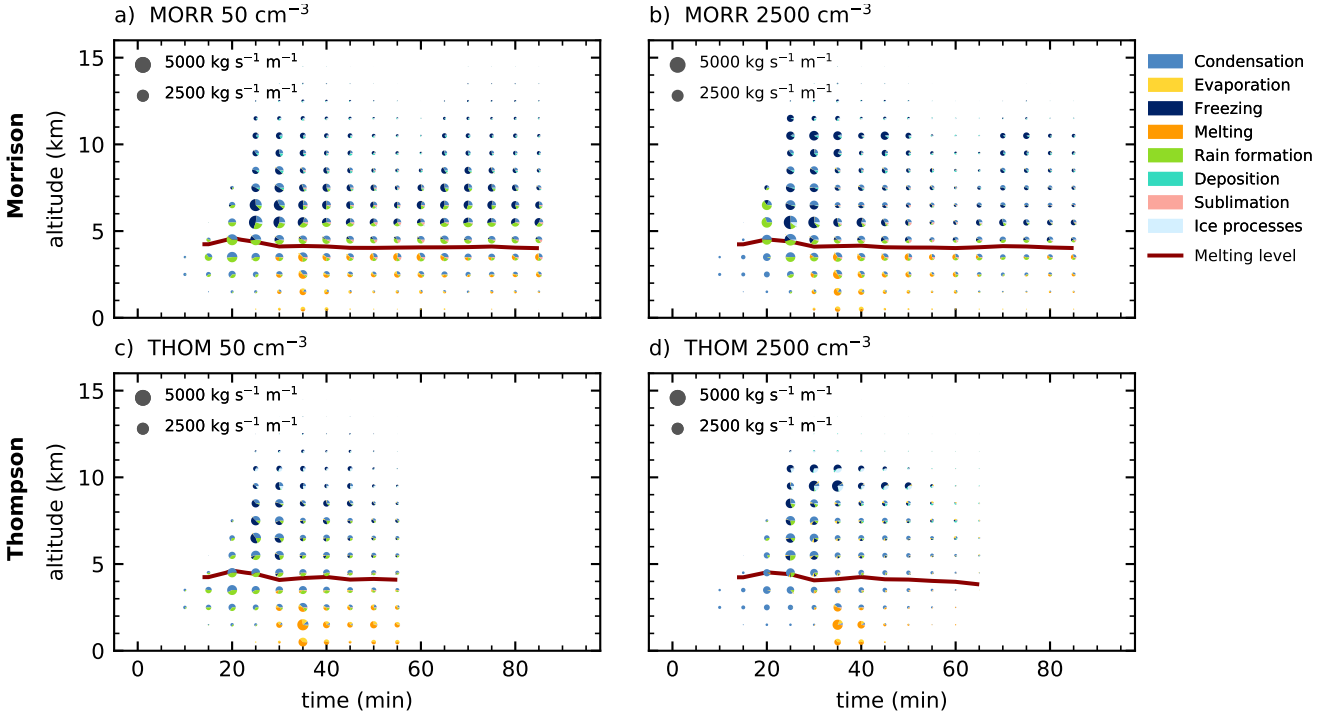

Figure 13. Temporal evolution of the microphysical process rates in CASE2 for the most clean (left) and most polluted (right) simulations and the two bulk microphysics schemes (Morrison: top, Thompson: bottom). The pie charts denote the different groups of microphysical process rates with the area proportional to the sum of the microphysical process rates in the specific altitude interval inside the cloud volume.

heights in the polluted case using the Morrison microphysics scheme. For the Thompson microphysics scheme, the formation of rain is decreased and shifted to higher levels in the model under polluted conditions. Furthermore, the freezing and riming processes predominantly occur at higher altitudes than in the clean case for both bulk microphysics schemes.

In line with these changes to the microphysical process rates, the evolution of the cloud mass in CASE2 (Fig. 14) is smaller than in CASE1 for the two bulk microphysics schemes, with about half as much hydrometeor mass in the cloud up to about $5 \cdot 10^9$ kg. The ice phase is more dominant, with the liquid phase of the cloud only accounting for less than a quarter of the total cloud mass. The simulation with the spectral bin microphysics scheme shows a larger cloud mass than the two bulk schemes for this case, only about 30% smaller than in CASE1 (Fig. 14 a,b,c), which includes much more frozen hydrometeor mass than the two bulk microphysics schemes (Fig. 14 d,e,f), while liquid-phase mass is similar between the three microphysics schemes (Fig. 14 g,h,i).

The effects of a variation of CDNC are quite similar to the ones seen in CASE1 for the two bulk microphysics schemes (Fig. 14 a,b). The simulations with the Morrison scheme show a relatively small decrease in cloud mass, while cloud mass increased by about 15% for the Thompson microphysics scheme. These changes are almost entirely due to changes in the ice phase of the clouds with insignificant effects of a variation in the liquid phase (Fig. 14 g,h) for both bulk schemes. The

Atmos. Chem. Phys. Discuss., https://doi.org/10.5194/acp-2018-609
Manuscript under review for journal Atmos. Chem. Phys.
Discussion started: 30 August 2018

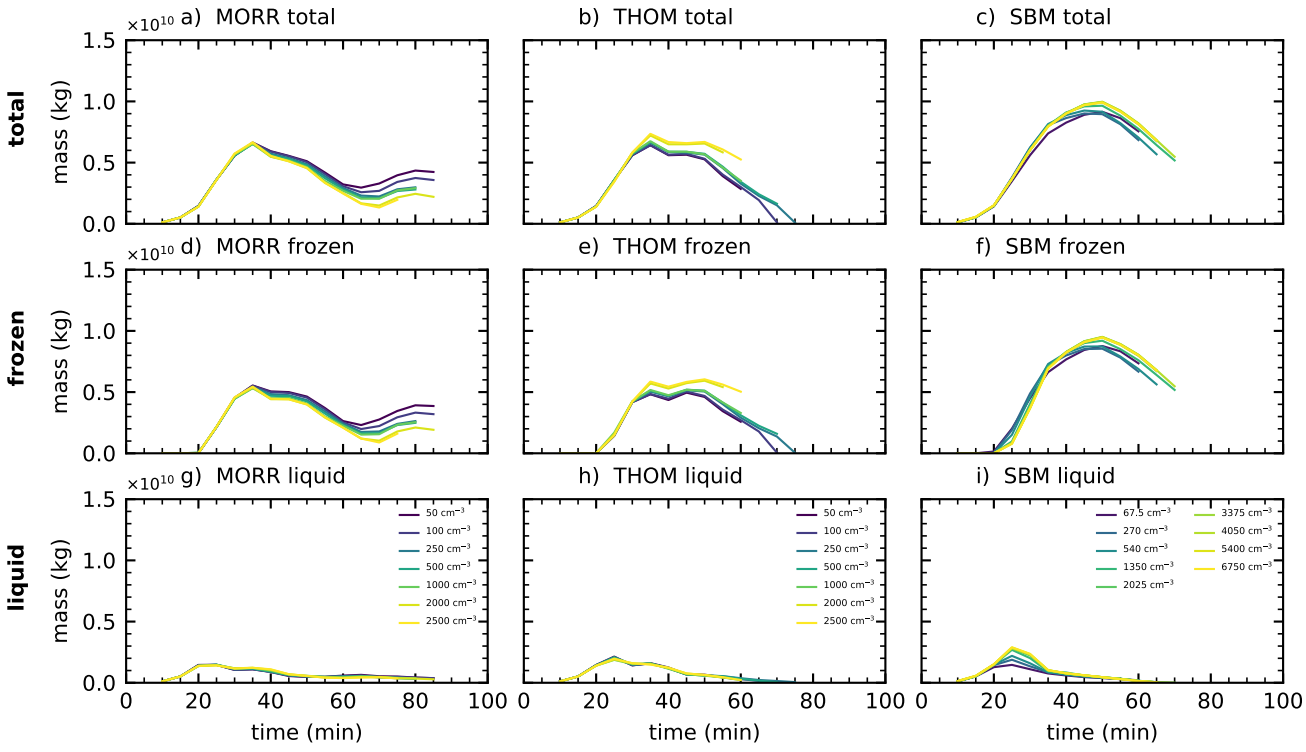

Figure 14. Total water mass, liquid water mass and ice water mass in the dominant tracked cell for the three different microphysics schemes (Morrison: left, Thompson: middle, SBM: right) in CASE2.

simulations with the spectral bin microphysics scheme, however, show an opposite response compared to CASE1 with an increase of cloud mass of a similar magnitude as the variation in the two bulk microphysics schemes (Fig. 14 c), which is dominated by changes in the ice phase (Fig. 14 f). There is a significant increase of almost 50% in cloud liquid mass in the earlier stages of the cloud evolution (Fig. 14 i) around 25 minutes simulation time between the most clean and the most polluted simulation with the SBM scheme. This coincides with a delayed evolution of the ice phase during that period of the developing cloud.

The changes in the altitude of the centre of gravity show less clear relationships to changes in the aerosol proxies CDNC/CCN in this case for the two bulk microphysics scheme. The Morrison scheme (Fig. 15 a,d,g) has the strongest variation in the time evolution of the altitude of the centre of gravity but generally shows a decrease of the altitude for both the liquid and the ice phase in the cloud. In the Thompson scheme (Fig. 15 b,e,h) increased CDNC leads to an increase in the height of the centre of gravity of the total cloud and both the individual phases. Similarly, increasing CCN in the spectral-bin microphysics scheme (Fig. 15 c,f,i) leads to a strong increase in the altitude of the cloud mass and the individual phases, with the COG of total mass about 1.5 km higher in the most polluted case (6750 cm^{-3}) compared to the clean case (67.5 cm^{-3}) and and even stronger

Atmos. Chem. Phys. Discuss., https://doi.org/10.5194/acp-2018-609
Manuscript under review for journal Atmos. Chem. Phys.
Discussion started: 30 August 2018

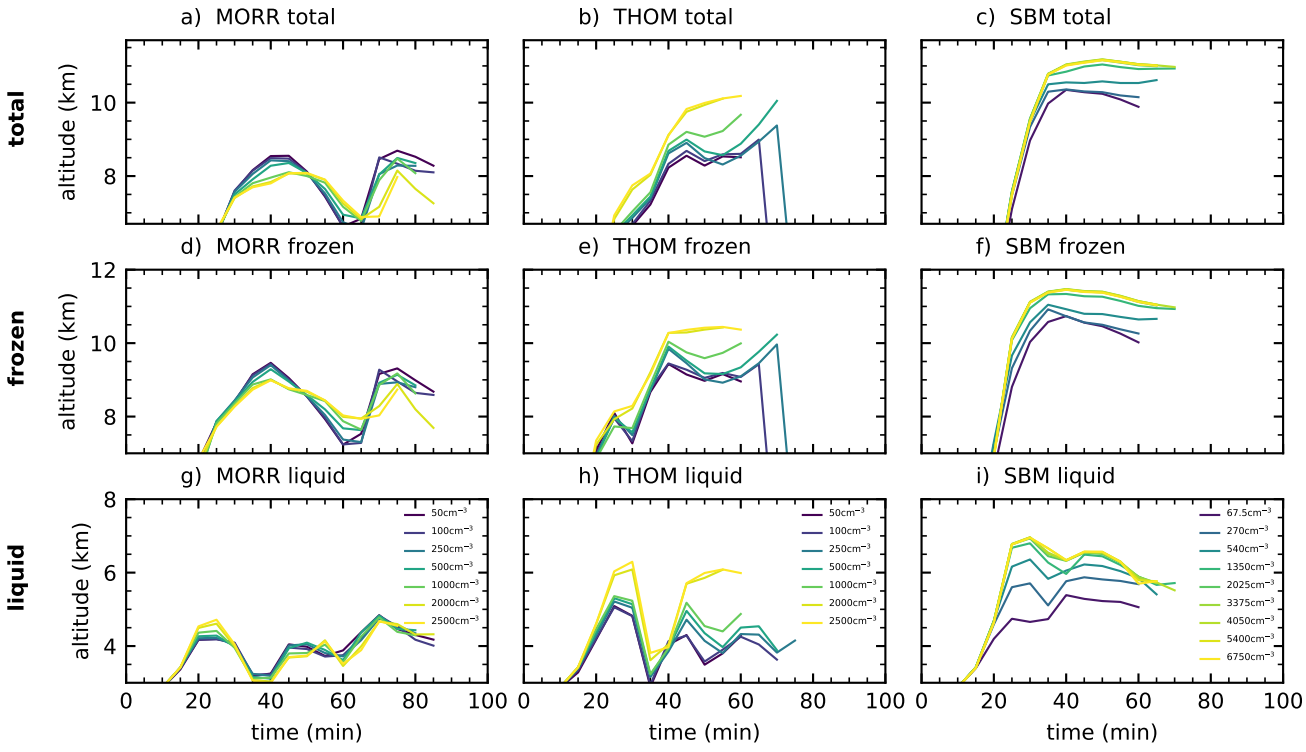

Figure 15. Altitude of the centre of gravity of the cloud and the individual phases for the three different microphysics schemes (Morrison: left, Thompson: middle, SBM: right) in CASE2.

increase of up to 2 km increase in the liquid phase. All the SBM simulations with a higher CCN value than about 1500 cm^{-3} lead to relatively similar results, which means that the aerosol effects saturate at this value.

4 Conclusions

We investigated the effects of changes in cloud droplet number concentration (CDNC) and cloud condensation nuclei (CCN) concentrations on the development of idealised simulations of deep convection to test proposed aerosol effects on deep convection e.g. due to different mechanisms of convective invigoration (Rosenfeld et al., 2008; Lebo and Seinfeld, 2011; Fan et al., 2013; Grabowski and Morrison, 2016). A combination of cell tracking and detailed process rate diagnostics were used to investigate the evolution and structure of the microphysical processes in individual deep convective cells. We used three different cloud microphysics schemes (two bulk schemes and one bin scheme) to investigate how the choice of microphysics scheme affects these results. By covering a wide range of values of CDNC/CCN representative of conditions from very clean to very polluted, we were able to look for consistent responses of the clouds to changes in these aerosol proxies and thus go beyond a simple comparison of just clean and polluted conditions.

An increase in cloud droplet number concentration from values representing clean conditions (CDNC=50 cm^{-3}) to strongly polluted conditions (CDNC=2500 cm^{-3}) leads to a shift of freezing processes to higher levels in both bulk microphysics schemes. Detailed analyses of the individual process rates confirmed that this is indeed related to a shift from freezing of rain to freezing of cloud droplets and a decrease in riming of rain drops due to larger amounts of liquid water in the form of cloud droplets instead of rain. This in turn can be related to the changes in autoconversion and accretion in the warm-phase region of the cloud. This is in line with the first step of the mechanisms proposed for convective invigoration of deep convection due to an increase in aerosols acting as CCN (e.g. Rosenfeld et al., 2008; Lebo and Seinfeld, 2011; Altaratz et al., 2014; Fan et al., 2013). These changes are concurrent and linked to changes in the prevailing hydrometeors in the different parts of the clouds. All microphysics schemes showed a strong increase of cloud droplet mixing ratio at the expense of rain drops for increased CDNC. In the ice phase of the clouds, there is a clear shift from mainly graupel or hail in the low-CDNC simulations to larger fractions of snow and ice crystals in the high-CDNC simulations. It was also shown that melting of frozen hydrometeors contributes significantly to the formation of rain drops, especially under high CDNC conditions.

However, there is no evident change in the integrated latent heat from an absolute increase in the freezing and riming to constitute a significant convective invigoration based on increased freezing as suggested in Rosenfeld et al. (2008). Since the cases of intense deep convection studied here are characterised by a near complete transfer of condensate mass into the ice phase and dominated by cold rain precipitation processes for all different CDNC/CCN values chosen, there is only a very limited potential for this cold-phase invigoration pathway.

A more detailed analysis of the different components of the latent heating for the two bulk microphysics schemes shows a complex superposition of changes to the different phase changes in the tracked cells. Condensation and evaporation are the largest contributions to latent heating and cooling in the cloud. The changes in these two processes due to changes in the aerosol proxies CDNC and CCN, are comparatively small, except for the changes in the evaporation of rain. This is to be expected as condensation and evaporation of cloud droplets in the two bulk microphysics schemes are represented using saturation adjustment, which does not include the effect of changes in cloud drop radius on the condensation and evaporation processes. Saturation adjustment has the potential to mask the effects of aerosols in highly supersaturated strong convective updrafts as described e.g. in Lebo et al. (2012) and Fan et al. (2018). Lebo et al. (2012) argue that saturation adjustment, as used in both bulk microphysics schemes in this study, leads to an artificial increase in condensation in the lower levels of the clouds, which would limit the effects of aerosol concentrations on buoyancy in mid and high levels.

There are significant differences between the two bulk schemes in the profiles of sublimation and deposition as well as in the response of these processes to changes in CDNC. This can be attributed to different parameter values used by the different schemes, especially to the fact that deposition onto graupel hydrometeors is not allowed to occur in the Thompson microphysics scheme. The analysis of cloud with respect to the total cloud mass and the altitude of the centre of gravity showed some contrasting results between the different microphysics schemes. There is a clear signal of a lifting of all parts of the clouds to higher altitude under polluted conditions, which can be interpreted as a form of convective invigoration. However, the analysis of cloud mass revealed opposing trends in the response between the three microphysics schemes. There is no clear pattern in the different responses to CDNC/CCN with regard to these bulk cloud properties, with variations between the two

bulk microphysics schemes often as large as between the bulk schemes and the spectral bin microphysics scheme, which confirms the strong differences between microphysics schemes found in previous studies (White et al., 2017; Khain et al., 2015; Lebo et al., 2012).

The results for the first case (CASE1), based on Weisman and Klemp (1982, 1984), are supported by the analysis of a second idealised supercell case (CASE2), based on Kumjian et al. (2010); Dawson et al. (2013). The microphysical process rate diagnostics revealed similar changes in rain formation and the altitude of freezing and riming processes for the two bulk microphysics schemes in this second case. All three microphysics schemes showed that the effects of a variation of CDNC or CCN clearly saturates above a threshold value. Variations above a CDNC of around $2000\,\mathrm{cm}^{-3}$ in the bulk schemes and a CCN concentration above $1500\,\mathrm{cm}^{-3}$ in the bin microphysics scheme do not lead to any further changes in the convective clouds, with regard to cloud condensate mass or altitude.

The pathway analysis developed for this study also includes the process rates for the number concentrations of the different hydrometeors. This includes processes like ice multiplication that could play an important role to better understand some of the possible pathways of aerosol effects on convective clouds (Fan et al., 2013, 2016).

This work focused on the analysis of microphysical pathways of aerosol effects on deep convective clouds in an idealised framework To test the robustness of the results under realistic scenarios, including potential buffering mechanisms, we are currently applying our analysis framework to large case study simulations of isolated convection over the area around Houston, Texas as part of the ACPC initiative (Aerosol, Cloud, Precipitation, and Climate Working Group, http://www.acpcinitiative.org) . We apply the cell tracking algorithm and the analysis of detailed process rates output developed in this study for a range of different cloud resolving models and contrasting aerosol conditions. In these simulations, the individual deep convective clouds in the cloud field evolve and interact freely, which allows for a thorough analysis of important aspects such as the impact of aerosol conditions on the cell lifetimes or on the statistics of the cloud size spectrum. The introduction of parameters describing the entire convective cell such as cloud mass and the position of the centre of gravity can contribute to a meaningful analysis cloud field simulations with a large number of individual clouds.

The understanding of the detailed structure of microphysical processes in individually tracked deep convective clouds and the analysis of the pathways through which aerosol perturbations affect the deep convective clouds advances our understanding of aerosol-cloud interactions. This can be used to inform the parametrisation of microphysical processes and aerosol-convection interactions in global climate models. Recent developments in the use of global cloud resolving models in climate research (e.g. Ban et al., 2014; Seiki et al., 2014; Sato et al., 2018) further motivate a detailed understanding of the pathways of aerosol effects on convective clouds and the uncertainties in their representation in numerical models.

A1 Convective cell tracking

The tracking algorithm tracks individual convective cells and their volume based on the model output fields of vertical velocity and total condensate mixing ratio. The tracking of maxima in the column vertical velocity field is performed using trackpy (Allan et al., 2016). The algorithm from trackpy that is used to identify the updraft features requires an initial assumption for the size of the tracked object. We chose a diameter of $15\,\mathrm{km}$ to represent the large convective updrafts in the supercell cases.

Tracked updrafts are required to exist for 6 output timesteps, i.e. 30 minutes, to be included in the analysis, which helps to exclude spurious features in vertical velocity and thus focus on the analysis of properly developed deep convective cells. We extrapolate by two timesteps at the beginning and the end of each tracked trajectory to include a representation of the initial development of the convective clouds and the evolution after the weakening of the central updraft.

The volume of the convective clouds is determined by a watershedding algorithm using a fixed threshold to determine the extent of the individual clouds based on the tracked updrafts. We use a threshold of $1\,\mathrm{g\,cm^{-3}}$ for the total water content in this study and a variation of this threshold by an order of magnitude to $0.1\,\mathrm{g\,cm^{-3}}$ showed that choosing a lower threshold did not significantly change the cloud volume and cloud mass or any of the more detailed process analyses.

A2 Microphysics schemes and process rate diagnostics

Table A1 and Table A2 give an overview of the microphysical process rates for the hydrometeor masses as they are implemented in the two microphysics schemes (Morrison et al., 2009; Thompson et al., 2008). In the Morrison microphysics scheme as used in this study, the autoconversion of cloud droplets and accretion by rain are parametrised based on Khairoutdinov and Kogan (2000). Ice nucleation follows Rasmussen et al. (2002); Cooper (1986). The Thompson scheme applies an autoconversion parametrisation based on Berry and Reinhardt (1974). Freezing follows Bigg (1953), Cooper (1986) and Koop et al. (2000).

Author contributions. M.H., B.W., L.L. and P.S. designed the experiment, M.H. and B.W. implemented the microphysical pathway analysis in WRF, M.H. set up the simulations and developed the data analysis including the tracking algorithm, M.H. wrote the manuscript and B.W., P.S. and L.L contributed to the analysis and the manuscript.

Competing interests. The authors declare that they have no conflict of interest.

Code availability. The WRF model is publicly available and can be downloaded from http://www2.mmm.ucar.edu/wrf/users/download/get_sources.html. The code of the modified WRF model with the microphysical pathway diagnostics for the two bulk microphysics schemes and the additional second supercell case is available from the authors on request along with postprocessing code for the process rate analysis in python. The tracking algorithm applied in this study is hosted on github (https://github.com/mheikenfeld/cloudtrack). It makes use of trackpy (Allan et al., 2016), which is available on github (https://github.com/soft-matter/trackpy).

Acknowledgements. M.H acknowledges funding from the NERC Oxford DTP in Environmental Research (NE/L002612/1). The research leading to these results has received funding from the European Union's Seventh Framework Programme (FP7/2007-2013) project BACCHUS under grant agreement n° 603445 (M.H., P.S. and L.L). The authors acknowledge funding from the European Research Council project ACCLAIM (P.S. and B.W) under grand agreement n° 28002 from the European Union's Seventh Framework Programme (FP7/2007-

2013) . P.S. acknowledges funding from the European Research Council project RECAP under the European Union's Horizon 2020 research and innovation programme with grant agreement 724602.

The authors would like to acknowledge the use of the University of Oxford Advanced Research Computing (ARC) facility (doi:10.5281/zenodo.22558) in carrying out this work.

We want to thank Hugh Morrison and Greg Thompson for important discussions about the two bulk microphysics schemes used in the study and Matthew Christensen for helpful comments on the manuscript.

References

Allan, D., Caswell, T., Keim, N., and van der Wel, C.: Trackpy: Trackpy v0.3.2, Tech. rep., Zenodo, https://doi.org/10.5281/zenodo.60550, 2016.

Altaratz, O., Koren, I., Remer, L. A., and Hirsch, E.: Review: Cloud Invigoration by Aerosols—Coupling between Microphysics and Dynamics, Atmospheric Research, 140–141, 38–60, https://doi.org/10.1016/j.atmosres.2014.01.009, 2014.

Andreae, M. O., Rosenfeld, D., Artaxo, P., Costa, A. A., Frank, G. P., Longo, K. M., and Silva-Dias, M. a. F.: Smoking Rain Clouds over the Amazon, Science, 303, 1337–1342, https://doi.org/10.1126/science.1092779, 2004.

Ban, N., Schmidli, J., and Schär, C.: Evaluation of the Convection-Resolving Regional Climate Modeling Approach in Decade-Long Simulations, Journal of Geophysical Research: Atmospheres, 119, 7889–7907, https://doi.org/10.1002/2014JD021478, 2014.

Berry, E. X. and Reinhardt, R. L.: An Analysis of Cloud Drop Growth by Collection Part II. Single Initial Distributions, Journal of the Atmospheric Sciences, 31, 1825–1831, https://doi.org/10.1175/1520-0469(1974)031<1825:AAOCDG>2.0.CO;2, 1974.

Bigg, E. K.: The Supercooling of Water, Proceedings of the Physical Society. Section B, 66, 688, https://doi.org/10.1088/0370-1301/66/8/309, 1953.

Chang, D., Cheng, Y., Reutter, P., Trentmann, J., Burrows, S. M., Spichtinger, P., Nordmann, S., Andreae, M. O., Pöschl, U., and Su, H.: Comprehensive Mapping and Characteristic Regimes of Aerosol Effects on the Formation and Evolution of Pyro-Convective Clouds, Atmos. Chem. Phys., 15, 10 325–10 348, https://doi.org/10.5194/acp-15-10325-2015, 2015.

Chen, Q., Koren, I., Altaratz, O., Heiblum, R. H., Dagan, G., and Pinto, L.: How Do Changes in Warm-Phase Microphysics Affect Deep Convective Clouds?, Atmos. Chem. Phys., 17, 9585–9598, https://doi.org/10.5194/acp-17-9585-2017, 2017.

Cooper, W. A.: Ice Initiation in Natural Clouds, in: Precipitation Enhancement—A Scientific Challenge, Meteorological Monographs, pp. 29–32, American Meteorological Society, Boston, MA, https://doi.org/10.1007/978-1-935704-17-1_4, 1986.

Dagan, G., Koren, I., and Altaratz, O.: Aerosol Effects on the Timing of Warm Rain Processes, Geophysical Research Letters, 42, 2015GL063 839, https://doi.org/10.1002/2015GL063839, 2015.

Dagan, G., Koren, I., Altaratz, O., and Heiblum, R. H.: Time-Dependent, Non-Monotonic Response of Warm Convective Cloud Fields to Changes in Aerosol Loading, Atmos. Chem. Phys., 17, 7435–7444, https://doi.org/10.5194/acp-17-7435-2017, 2017.

Dagan, G., Koren, I., and Altaratz, O.: Quantifying the Effect of Aerosol on Vertical Velocity and Effective Terminal Velocity in Warm Convective Clouds, Atmos. Chem. Phys., 18, 6761–6769, https://doi.org/10.5194/acp-18-6761-2018, 2018.

Dawe, J. T. and Austin, P. H.: Statistical Analysis of an LES Shallow Cumulus Cloud Ensemble Using a Cloud Tracking Algorithm, Atmos. Chem. Phys., 12, 1101–1119, https://doi.org/10.5194/acp-12-1101-2012, 2012.

Dawson, D. T., Mansell, E. R., Jung, Y., Wicker, L. J., Kumjian, M. R., and Xue, M.: Low-Level ZDR Signatures in Supercell Forward Flanks: The Role of Size Sorting and Melting of Hail, Journal of the Atmospheric Sciences, 71, 276–299, https://doi.org/10.1175/JAS-D-13-0118.1, 2013.

Emanuel, K. A.: Atmospheric Convection, Oxford University Press, 1994.

Fan, J., Rosenfeld, D., Ding, Y., Leung, L. R., and Li, Z.: Potential Aerosol Indirect Effects on Atmospheric Circulation and Radiative Forcing through Deep Convection, Geophysical Research Letters, 39, L09 806, https://doi.org/10.1029/2012GL051851, 2012.

Fan, J., Leung, L. R., Rosenfeld, D., Chen, Q., Li, Z., Zhang, J., and Yan, H.: Microphysical Effects Determine Macrophysical Response for Aerosol Impacts on Deep Convective Clouds, Proceedings of the National Academy of Sciences of the United States of America, 110, E4581–E4590, https://doi.org/10.1073/pnas.1316830110, 2013.

Fan, J., Wang, Y., Rosenfeld, D., and Liu, X.: Review of Aerosol–Cloud Interactions: Mechanisms, Significance, and Challenges, Journal of the Atmospheric Sciences, 73, 4221–4252, https://doi.org/10.1175/JAS-D-16-0037.1, 2016.

Fan, J., Rosenfeld, D., Zhang, Y., Giangrande, S. E., Li, Z., Machado, L. A. T., Martin, S. T., Yang, Y., Wang, J., Artaxo, P., Barbosa, H. M. J., Braga, R. C., Comstock, J. M., Feng, Z., Gao, W., Gomes, H. B., Mei, F., Pöhlker, C., Pöhlker, M. L., Pöschl, U., and de Souza, R. A. F.: Substantial Convection and Precipitation Enhancements by Ultrafine Aerosol Particles, Science, 359, 411–418, https://doi.org/10.1126/science.aan8461, 2018.

Gettelman, A.: Putting the Clouds Back in Aerosol–cloud Interactions, Atmos. Chem. Phys., 15, 12 397–12 411, https://doi.org/10.5194/acp-15-12397-2015, 2015.

Glassmeier, F. and Lohmann, U.: Constraining Precipitation Susceptibility of Warm-, Ice-, and Mixed-Phase Clouds with Microphysical Equations, Journal of the Atmospheric Sciences, 73, 5003–5023, https://doi.org/10.1175/JAS-D-16-0008.1, 2016.

Grabowski, W. W. and Morrison, H.: Untangling Microphysical Impacts on Deep Convection Applying a Novel Modeling Methodology. Part II: Double-Moment Microphysics, Journal of the Atmospheric Sciences, 73, 3749–3770, https://doi.org/10.1175/JAS-D-15-0367.1, 2016.

Guo, H., Golaz, J.-C., Donner, L. J., Wyman, B., Zhao, M., and Ginoux, P.: CLUBB as a Unified Cloud Parameterization: Opportunities and Challenges, Geophysical Research Letters, 42, 4540–4547, https://doi.org/10.1002/2015GL063672, 2015.

Heiblum, R. H., Altaratz, O., Koren, I., Feingold, G., Kostinski, A. B., Khain, A. P., Ovchinnikov, M., Fredj, E., Dagan, G., Pinto, L., Yaish, R., and Chen, Q.: Characterization of Cumulus Cloud Fields Using Trajectories in the Center of Gravity versus Water Mass Phase Space: 2. Aerosol Effects on Warm Convective Clouds, Journal of Geophysical Research: Atmospheres, 121, 2015JD024 193, https://doi.org/10.1002/2015JD024193, 2016a.

Heiblum, R. H., Altaratz, O., Koren, I., Feingold, G., Kostinski, A. B., Khain, A. P., Ovchinnikov, M., Fredj, E., Dagan, G., Pinto, L., Yaish, R., and Chen, Q.: Characterization of Cumulus Cloud Fields Using Trajectories in the Center of Gravity versus Water Mass Phase Space: 1. Cloud Tracking and Phase Space Description, Journal of Geophysical Research: Atmospheres, 121, 2015JD024 186, https://doi.org/10.1002/2015JD024186, 2016b.

Heus, T. and Seifert, A.: Automated Tracking of Shallow Cumulus Clouds in Large Domain, Long Duration Large Eddy Simulations, Geosci. Model Dev., 6, 1261–1273, https://doi.org/10.5194/gmd-6-1261-2013, 2013.

Igel, A. L., Igel, M. R., and van den Heever, S. C.: Make It a Double? Sobering Results from Simulations Using Single-Moment Microphysics Schemes, Journal of the Atmospheric Sciences, 72, 910–925, https://doi.org/10.1175/JAS-D-14-0107.1, 2014.

Kalina, E. A., Friedrich, K., Morrison, H., and Bryan, G. H.: Aerosol Effects on Idealized Supercell Thunderstorms in Different Environments, Journal of the Atmospheric Sciences, 71, 4558–4580, https://doi.org/10.1175/JAS-D-14-0037.1, 2014.

Khain, A. and Lynn, B.: Simulation of a Supercell Storm in Clean and Dirty Atmosphere Using Weather Research and Forecast Model with Spectral Bin Microphysics, Journal of Geophysical Research: Atmospheres, 114, D19 209, https://doi.org/10.1029/2009JD011827, 2009.

Khain, A., Pokrovsky, A., Pinsky, M., Seifert, A., and Phillips, V.: Simulation of Effects of Atmospheric Aerosols on Deep Turbulent Convective Clouds Using a Spectral Microphysics Mixed-Phase Cumulus Cloud Model. Part I: Model Description and Possible Applications, Journal of the Atmospheric Sciences, 61, 2963–2982, https://doi.org/10.1175/JAS-3350.1, 2004.

Khain, A., Rosenfeld, D., Pokrovsky, A., Blahak, U., and Ryzhkov, A.: The Role of CCN in Precipitation and Hail in a Mid-Latitude Storm as Seen in Simulations Using a Spectral (Bin) Microphysics Model in a 2D Dynamic Frame, Atmospheric Research, 1, 129–146, https://doi.org/10.1016/j.atmosres.2010.09.015, 2011.

Khain, A. P., Phillips, V., Benmoshe, N., and Pokrovsky, A.: The Role of Small Soluble Aerosols in the Microphysics of Deep Maritime Clouds, Journal of the Atmospheric Sciences, 69, 2787–2807, https://doi.org/10.1175/2011JAS3649.1, 2012.

Khain, A. P., Beheng, K. D., Heymsfield, A., Korolev, A., Krichak, S. O., Levin, Z., Pinsky, M., Phillips, V., Prabhakaran, T., Teller, A., van den Heever, S. C., and Yano, J.-I.: Representation of Microphysical Processes in Cloud-Resolving Models: Spectral (Bin) Microphysics versus Bulk Parameterization, Reviews of Geophysics, 53, 2014RG000 468, https://doi.org/10.1002/2014RG000468, 2015.

Khairoutdinov, M. and Kogan, Y.: A New Cloud Physics Parameterization in a Large-Eddy Simulation Model of Marine Stratocumulus, Monthly Weather Review, 128, 229–243, https://doi.org/10.1175/1520-0493(2000)128<0229:ANCPPI>2.0.CO;2, 2000.

Kipling, Z., Stier, P., Labbouz, L., and Wagner, T.: Dynamic Subgrid Heterogeneity of Convective Cloud in a Global Model: Description and Evaluation of the Convective Cloud Field Model (CCFM) in ECHAM6–HAM2, Atmos. Chem. Phys., 17, 327–342, https://doi.org/10.5194/acp-17-327-2017, 2017.

Koop, T., Luo, B., Tsias, A., and Peter, T.: Water Activity as the Determinant for Homogeneous Ice Nucleation in Aqueous Solutions, Nature, 406, 611–614, https://doi.org/10.1038/35020537, 2000.

Koren, I., Altaratz, O., Feingold, G., Levin, Z., and Reisin, T.: Cloud's Center of Gravity – a Compact Approach to Analyze Convective Cloud Development, Atmos. Chem. Phys., 9, 155–161, https://doi.org/10.5194/acp-9-155-2009, 2009.

Koren, I., Remer, L. A., Altaratz, O., Martins, J. V., and Davidi, A.: Aerosol-Induced Changes of Convective Cloud Anvils Produce Strong Climate Warming, Atmos. Chem. Phys., 10, 5001–5010, https://doi.org/10.5194/acp-10-5001-2010, 2010.

Kumjian, M. R., Ryzhkov, A. V., Melnikov, V. M., and Schuur, T. J.: Rapid-Scan Super-Resolution Observations of a Cyclic Supercell with a Dual-Polarization WSR-88D, Monthly Weather Review, 138, 3762–3786, https://doi.org/10.1175/2010MWR3322.1, 2010.

Labbouz, L., Kipling, Z., Stier, P., and Protat, A.: How Well Can We Represent the Spectrum of Convective Clouds in a Climate Model? Comparisons between Internal Parameterization Variables and Radar Observations, Journal of the Atmospheric Sciences, 75, 1509–1524, https://doi.org/10.1175/JAS-D-17-0191.1, 2018.

Lebo, Z. J. and Seinfeld, J. H.: Theoretical Basis for Convective Invigoration Due to Increased Aerosol Concentration, Atmos. Chem. Phys., 11, 5407–5429, https://doi.org/10.5194/acp-11-5407-2011, 2011.

Lebo, Z. J., Morrison, H., and Seinfeld, J. H.: Are Simulated Aerosol-Induced Effects on Deep Convective Clouds Strongly Dependent on Saturation Adjustment?, Atmos. Chem. Phys., 12, 9941–9964, https://doi.org/10.5194/acp-12-9941-2012, 2012.

Lohmann, U. and Feichter, J.: Global Indirect Aerosol Effects: A Review, Atmos. Chem. Phys., 5, 715–737, https://doi.org/10.5194/acp-5-715-2005, 2005.

Lynn, B. H., Khain, A. P., Dudhia, J., Rosenfeld, D., Pokrovsky, A., and Seifert, A.: Spectral (Bin) Microphysics Coupled with a Mesoscale Model (MM5). Part I: Model Description and First Results, Monthly Weather Review, 133, 44–58, https://doi.org/10.1175/MWR-2840.1, 2005a.

Lynn, B. H., Khain, A. P., Dudhia, J., Rosenfeld, D., Pokrovsky, A., and Seifert, A.: Spectral (Bin) Microphysics Coupled with a Mesoscale Model (MM5). Part II: Simulation of a CaPE Rain Event with a Squall Line, Monthly Weather Review, 133, 59–71, https://doi.org/10.1175/MWR-2841.1, 2005b.

Malavelle, F. F., Haywood, J. M., Jones, A., Gettelman, A., Clarisse, L., Bauduin, S., Allan, R. P., Karset, I. H. H., Kristjánsson, J. E., Oreopoulos, L., Cho, N., Lee, D., Bellouin, N., Boucher, O., Grosvenor, D. P., Carslaw, K. S., Dhomse, S., Mann, G. W., Schmidt, A., Coe, H., Hartley, M. E., Dalvi, M., Hill, A. A., Johnson, B. T., Johnson, C. E., Knight, J. R., O'Connor, F. M., Partridge, D. G., Stier, P., Myhre, G., Platnick, S., Stephens, G. L., Takahashi, H., and Thordarson, T.: Strong Constraints on Aerosol–cloud Interactions from Volcanic Eruptions, Nature, 546, 485–491, https://doi.org/10.1038/nature22974, 2017.

Morrison, H.: On the Robustness of Aerosol Effects on an Idealized Supercell Storm Simulated with a Cloud System-Resolving Model, Atmos. Chem. Phys., 12, 7689–7705, https://doi.org/10.5194/acp-12-7689-2012, 2012.

Morrison, H. and Milbrandt, J.: Comparison of Two-Moment Bulk Microphysics Schemes in Idealized Supercell Thunderstorm Simulations, Monthly Weather Review, 139, 1103–1130, https://doi.org/10.1175/2010MWR3433.1, 2010.

Morrison, H., Curry, J. A., and Khvorostyanov, V. I.: A New Double-Moment Microphysics Parameterization for Application in Cloud and Climate Models. Part I: Description, Journal of the Atmospheric Sciences, 62, 1665–1677, https://doi.org/10.1175/JAS3446.1, 2005.

Morrison, H., Thompson, G., and Tatarskii, V.: Impact of Cloud Microphysics on the Development of Trailing Stratiform Precipitation in a Simulated Squall Line: Comparison of One- and Two-Moment Schemes, Monthly Weather Review, 137, 991–1007, https://doi.org/10.1175/2008MWR2556.1, 2009.

Naylor, J. and Gilmore, M. S.: Convective Initiation in an Idealized Cloud Model Using an Updraft Nudging Technique, Monthly Weather Review, 140, 3699–3705, https://doi.org/10.1175/MWR-D-12-00163.1, 2012.

Rasmussen, R. M., Geresdi, I., Thompson, G., Manning, K., and Karplus, E.: Freezing Drizzle Formation in Stably Stratified Layer Clouds: The Role of Radiative Cooling of Cloud Droplets, Cloud Condensation Nuclei, and Ice Initiation, Journal of the Atmospheric Sciences, 59, 837–860, https://doi.org/10.1175/1520-0469(2002)059<0837:FDFISS>2.0.CO;2, 2002.

Rosenfeld, D., Lohmann, U., Raga, G. B., O'Dowd, C. D., Kulmala, M., Fuzzi, S., Reissell, A., and Andreae, M. O.: Flood or Drought: How Do Aerosols Affect Precipitation?, Science, 321, 1309–1313, https://doi.org/10.1126/science.1160606, 2008.

Rosenfeld, D., Sherwood, S., Wood, R., and Donner, L.: Climate Effects of Aerosol-Cloud Interactions, Science, 343, 379–380, https://doi.org/10.1126/science.1247490, 2014.

Sato, Y., Goto, D., Michibata, T., Suzuki, K., Takemura, T., Tomita, H., and Nakajima, T.: Aerosol Effects on Cloud Water Amounts Were Successfully Simulated by a Global Cloud-System Resolving Model, Nature Communications, 9, 985, https://doi.org/10.1038/s41467-018-03379-6, 2018.

Schutgens, N. A. J. and Stier, P.: A Pathway Analysis of Global Aerosol Processes, Atmos. Chem. Phys., 14, 11 657–11 686, https://doi.org/10.5194/acp-14-11657-2014, 2014.

Seifert, A. and Beheng, K. D.: A Two-Moment Cloud Microphysics Parameterization for Mixed-Phase Clouds. Part 2: Maritime vs. Continental Deep Convective Storms, Meteorology and Atmospheric Physics, 92, 67–82, https://doi.org/10.1007/s00703-005-0113-3, 2006.

Seiki, T., Kodama, C., Noda, A. T., and Satoh, M.: Improvement in Global Cloud-System-Resolving Simulations by Using a Double-Moment Bulk Cloud Microphysics Scheme, Journal of Climate, 28, 2405–2419, https://doi.org/10.1175/JCLI-D-14-00241.1, 2014.

Skamarock, W. C., Klemp, J. B., Dudhia, J., Gill, D. O., Barker, D. M., Wang, W., and Powers, J. G.: A Description of the Advanced Research WRF Version 2, Tech. rep., DTIC Document, 2005.

Song, X. and Zhang, G. J.: Microphysics Parameterization for Convective Clouds in a Global Climate Model: Description and Single-Column Model Tests, Journal of Geophysical Research: Atmospheres, 116, https://doi.org/10.1029/2010JD014833, 2011.

Stevens, B. and Feingold, G.: Untangling Aerosol Effects on Clouds and Precipitation in a Buffered System, Nature, 461, 607–613, https://doi.org/10.1038/nature08281, 2009.

Stocker, T. F.: Climate Change 2013: The Physical Science Basis: Working Group I Contribution to the Fifth Assessment Report of the Intergovernmental Panel on Climate Change, Cambridge University Press, 2014.

Storer, R. L., van den Heever, S. C., and Stephens, G. L.: Modeling Aerosol Impacts on Convective Storms in Different Environments, Journal of the Atmospheric Sciences, 67, 3904–3915, https://doi.org/10.1175/2010JAS3363.1, 2010.

Sullivan, S. C., Lee, D., Oreopoulos, L., and Nenes, A.: Role of Updraft Velocity in Temporal Variability of Global Cloud Hydrometeor Number, Proceedings of the National Academy of Sciences, 113, 5791–5796, https://doi.org/10.1073/pnas.1514039113, 2016.

Tao, W.-K., Chen, J.-P., Li, Z., Wang, C., and Zhang, C.: Impact of Aerosols on Convective Clouds and Precipitation, Reviews of Geophysics, 50, RG2001, https://doi.org/10.1029/2011RG000369, 2012.

Terwey, W. D. and Rozoff, C. M.: Objective Convective Updraft Identification and Tracking: Part 1. Structure and Thermodynamics of Convection in the Rainband Regions of Two Hurricane Simulations, Journal of Geophysical Research: Atmospheres, 119, 6470–6496, https://doi.org/10.1002/2013JD020904, 2014.

Thompson, G., Rasmussen, R. M., and Manning, K.: Explicit Forecasts of Winter Precipitation Using an Improved Bulk Microphysics Scheme. Part I: Description and Sensitivity Analysis, Monthly Weather Review, 132, 519–542, https://doi.org/10.1175/1520-0493(2004)132<0519:EFOWPU>2.0.CO;2, 2004.

Thompson, G., Field, P. R., Rasmussen, R. M., and Hall, W. D.: Explicit Forecasts of Winter Precipitation Using an Improved Bulk Microphysics Scheme. Part II: Implementation of a New Snow Parameterization, Monthly Weather Review, 136, 5095–5115, https://doi.org/10.1175/2008MWR2387.1, 2008.

van der Walt, S., Schönberger, J. L., Nunez-Iglesias, J., Boulogne, F., Warner, J. D., Yager, N., Gouillart, E., and Yu, T.: Scikit-Image: Image Processing in Python, PeerJ, 2, e453, https://doi.org/10.7717/peerj.453, 2014.

Varble, A.: Erroneous Attribution of Deep Convective Invigoration to Aerosol Concentration, Journal of the Atmospheric Sciences, 75, 1351–1368, https://doi.org/10.1175/JAS-D-17-0217.1, 2018.

Weisman, M. L. and Klemp, J. B.: The Dependence of Numerically Simulated Convective Storms on Vertical Wind Shear and Buoyancy, Monthly Weather Review, 110, 504–520, 1982.

Weisman, M. L. and Klemp, J. B.: The Structure and Classification of Numerically Simulated Convective Stormsin Directionally Varying Wind Shears, Monthly Weather Review, 112, 2479–2498, 1984.

White, B., Gryspeerdt, E., Stier, P., Morrison, H., Thompson, G., and Kipling, Z.: Uncertainty from the Choice of Microphysics Scheme in Convection-Permitting Models Significantly Exceeds Aerosol Effects, Atmos. Chem. Phys., 17, 12 145–12 175, https://doi.org/10.5194/acp-17-12145-2017, 2017.

Zhang, K., Fu, R., Shaikh, M. J., Ghan, S., Wang, M., Leung, L. R., Dickinson, R. E., and Marengo, J.: Influence of Superparameterization and a Higher-Order Turbulence Closure on Rainfall Bias Over Amazonia in Community Atmosphere Model Version 5, Journal of Geophysical Research: Atmospheres, 122, 9879–9902, https://doi.org/10.1002/2017JD026576, 2017.

Atmos. Chem. Phys. Discuss., https://doi.org/10.5194/acp-2018-609
Manuscript under review for journal Atmos. Chem. Phys.
Discussion started: 30 August 2018

Atmospheric Chemistry and Physics Discussions

Table A1. Mass transfer process rates for the Morrison microphysics scheme (Morrison et al., 2009)

Variable	Description	from	to	Grouping
PCCN	Activation	vapour	droplets	Condensation
PCC	Condensation on droplets	vapour	droplets	
EPCC	Evaporation of droplets	droplets	vapour	Evaporation
PRE	Evaporation of rain	rain	vapour	
PRA	Accretion	droplets	rain	Rain formation
PRC	Autoconversion	droplets	rain	
MNUCCC	Contact freezing of droplets	droplets	ice	Freezing
MNUCCD	Primary ice nucleation	droplets	ice	
QICF	Instantaneous freezing of droplets	droplets	ice	
MNUCCR	Contact freezing of rain	rain	ice	
QGRF	Instantaneous freezing of rain	rain	graupel	
QNIRF	Instantaneous freezing of rain	rain	snow	
PSACWS	Riming on snow	droplets	snow	Riming
PSACWI	Riming on ice	droplets	ice	
PSACWG	Collection of droplets by graupel	droplets	graupel	
PGSACW	Collection of droplets by snow	droplets	graupel	
PRACS	Rain-snow collection	rain	snow	
PIACR	Ice-rain collision	rain	graupel	
PIACRS	Ice-rain collision	rain	snow	
PRACG	Collection of rain by graupel	rain	graupel	
PGRACS	Collection of rain by snow	rain	graupel	
QMULTG	Ice multiplication droplets and graupel	droplets	ice	
QMULTS	Ice multiplication droplets and snow	droplets	ice	
QMULTRG	Ice multiplication rain and graupel	rain	ice	
QMULTR	Ice multiplication rain and snow	rain	ice	
PGMLT	Graupel melting	graupel	rain	Melting
QIIM	Instantaneous melting of cloud ice	ice	droplets	
PSMLT	Snow Melting	snow	rain	
PRD	Deposition on ice	vapour	ice	Deposition
PRDS	Deposition on snow	vapour	snow	
PRDG	Deposition on graupel	vapour	graupel	
EPRDG	Sublimation of graupel	graupel	vapour	Sublimation
EVPMG	Graupel melting and evaporating	graupel	vapour	
EPRD	Sublimation of ice	ice	vapour	
EPRDS	Sublimation of snow	snow	vapour	
EVPMS	Snow melting and evaporating	snow	vapour	
PSACR	Collection of snow by rain	snow	graupel	
PRAI	Accretion of cloud ice by snow	ice	snow	Ice processes
PRCI	Autoconversion of cloud ice to snow	ice	snow	
PRACI	Ice-rain collection (ice to graupel)	ice	graupel	
PRACIS	Ice-rain collision (ice to snow)	ice	snow	

Atmos. Chem. Phys. Discuss., https://doi.org/10.5194/acp-2018-609
Manuscript under review for journal Atmos. Chem. Phys.
Discussion started: 30 August 2018

Atmospheric Chemistry and Physics Discussions

Table A2. Mass transfer process rates for the Thompson microphysics scheme (Thompson et al., 2008)

Variable	Description	from	to	Grouping
PRW_VCD	Condensation	vapour	droplets	Condensation
PRV_REV	Rain evaporation	vapour	droplets	Evaporation
E_PRW_VCD	Droplet evaporation	droplets	vapour	
PRR_WAU	Autoconversion	droplets	droplets	Rain formation
PRR_RCW	Accretion	droplets	rain	
PRI_WFZ	Freezing of cloud droplets	droplets	ice	Freezing
PRI_RFZ	Freezing of rain to ice	rain	ice	
PRI_IHA	Freezing of aqueous aerosols	droplets	ice	
PRG_RFZ	Freezing of rain to graupel	rain	graupel	
PRS_SCW	Collection of droplets by snow	droplets	snow	Riming
PRG_SCW	Collection of droplets by snow	droplets	snow	
PRG_RCG	Collection of rain by graupel	rain	graupel	
PRG_GCW	Collection of droplets by graupel	droplets	graupel	
PRS_RCS	Collection of snow by rain	snow	rain	Melting
PRR_RCI	Collection of ice by rain	ice	rain	
PRR_GML	Melting of graupel	graupel	rain	
PRI_RCI	Rain collection of ice	ice	rain	
PRR_RCS	Collection of snow by rain	snow	rain	
PRR_RCG	Collection of graupel by rain	rain	graupel	
PRS_SDE	Deposition on snow	vapour	snow	Deposition
PRS_IDE	Deposition on ice to snow	vapour	snow	
PRI_IDE	Deposition on ice	vapour	ice	
PRG_GDE	Deposition on graupel	vapour	graupel	
PRI_INU	Ice nucleation	vapour	ice	
E_PRS_SDE	Sublimation of snow	snow	vapour	Sublimation
E_PRI_IDE	Sublimation of ice	ice	vapour	
E_PRG_GDE	Sublimation of graupel	graupel	vapour	
PRS_SCI	Collection of ice by snow to graupel	ice	graupel	Ice processes
PRS_IHM	Hallet-Mossop process	snow	ice	
PRS_IAU	Autoconversion of ice to snow	ice	snow	
PRG_RCS	Collection of ice by snow	ice	graupel	
PRG_RCI	Collection of ice by rain	ice	graupel	
PRG_IHM	Hallet-Mossop process	graupel	ice	